Planetary transit candidates in CoRoT-LRc01 field

J. Cabrera, M. Fridlund, M. Ollivier, D. Gandolfi, S. Csizmadia, R. Alonso, S. Aigrain, A. Alapini, J.M. Almenara, P. Barge, et al.

A&A 506, 501–517 (2009)
DOI: 10.1051/0004-6361/200912684

Astronomy & Astrophysics
Special feature

The CoRoT space mission: early results

Planetary transit candidates in CoRoT-LRc01 field⋆

J. Cabrera[1,2], M. Fridlund[3], M. Ollivier[4], D. Gandolfi[5], Sz. Csizmadia[1], R. Alonso[6,7], S. Aigrain[8], A. Alapini[8], J.-M. Almenara[9], P. Barge[6], A. S. Bonomo[6,10], P. Bordé[4], F. Bouchy[11], H. Bruntt[12], L. Carone[13], S. Carpano[3], H. J. Deeg[9], R. De la Reza[14], M. Deleuil[6], R. Dvorak[15], A. Erikson[1], M. Gillon[16,7], P. Gondoin[3], E. W. Guenther[5], T. Guillot[17], M. Hartmann[5], A. Hatzes[5], G. Hebrard[11], L. Jorda[6], H. Lammer[18], A. Léger[4], A. Llebaria[6], C. Lovis[7], P. Magain[19], M. Mayor[7], T. Mazeh[20], C. Moutou[6], A. Ofir[21], M. Pätzold[13], F. Pepe[7], F. Pont[8], D. Queloz[7], M. Rabus[9], H. Rauer[1,22], C. Régulo[9,23], S. Renner[1,24,25], D. Rouan[12], B. Samuel[4], A. Santerne[6], J. Schneider[2], A. Shporer[20], B. Stecklum[5], B. Tingley[9], S. Udry[7], and G. Wuchterl[5]

[1] Institute of Planetary Research, German Aerospace Center, Rutherfordstrasse 2, 12489 Berlin, Germany
e-mail: juan.cabrera@dlr.de
[2] LUTH, Observatoire de Paris, CNRS, Université Paris Diderot, 5 place Jules Janssen, 92190 Meudon, France
[3] Research and Scientific Support Department, ESTEC/ESA, PO Box 299, 2200 AG Noordwijk, The Netherlands
[4] Institut d'Astrophysique Spatiale, Université Paris XI, 91405 Orsay, France
[5] Thüringer Landessternwarte, Sternwarte 5, Tautenburg 5, 07778 Tautenburg, Germany
[6] Laboratoire d'Astrophysique de Marseille, UMR 6110, CNRS/Université de Provence, 38 rue F. Joliot-Curie, 13388 Marseille, France
[7] Observatoire de Genève, Université de Genève, 51 chemin des Maillettes, 1290 Sauverny, Switzerland
[8] School of Physics, University of Exeter, Stocker Road, Exeter EX4 4QL, UK
[9] Instituto de Astrofísica de Canarias, E-38205 La Laguna, Tenerife, Spain
[10] INAF – Osservatorio Astrofisico di Catania, via S. Sofia 78, 95123 Catania, Italy
[11] Institut d'Astrophysique de Paris, Université Pierre & Marie Curie, 98bis Bd Arago, 75014 Paris, France
[12] LESIA, Observatoire de Paris-Meudon, 5 place Jules Janssen, 92195 Meudon, France
[13] Rheinisches Institut für Umweltforschung an der Universität zu Köln, Aachener Strasse 209, 50931, Germany
[14] Observatório Nacional, Rio de Janeiro, RJ, Brazil
[15] University of Vienna, Institute of Astronomy, Türkenschanzstr. 17, 1180 Vienna, Austria
[16] Institut d'Astrophysique et de Géophysique, Université de Liège, 17 Allée du 6 Août, Bât. B5C, Liège 1, Belgium
[17] Observatoire de la Côte d'Azur, Laboratoire Cassiopée, BP 4229, 06304 Nice Cedex 4, France
[18] Space Research Institute, Austrian Academy of Science, Schmiedlstr. 6, 8042 Graz, Austria
[19] University of Liège, Allée du 6 août 17, Sart Tilman, Liège 1, Belgium
[20] Wise Observatory, Tel Aviv University, Tel Aviv 69978, Israel
[21] School of Physics and Astronomy, Raymond and Beverly Sackler Faculty of Exact Sciences, Tel Aviv University, Tel Aviv, Israel
[22] Center for Astronomy and Astrophysics, TU Berlin, Hardenbergstr. 36, 10623 Berlin, Germany
[23] Dpto. de Astrofísica, Universidad de La Laguna, 38206 La Laguna, Tenerife, Spain
[24] Laboratoire d'Astronomie de Lille, Université de Lille 1, 1 impasse de l'Observatoire, 59000 Lille, France
[25] Institut de Mécanique Céleste et de Calcul des Ephémérides, UMR 8028 du CNRS, 77 avenue Denfert-Rochereau, 75014 Paris, France

Received 12 June 2009 / Accepted 27 July 2009

ABSTRACT

Aims. We present here the list of planetary transit candidates detected in the first long run observed by CoRoT: LRc01, towards the galactic center in the direction of Aquila, which lasted from May to October 2007.
Methods. we analyzed 3719 (33%) sources in the chromatic bands and 7689 in the monochromatic band. Instrumental noise and the stellar variability were treated with several detrending tools, on which subsequently several transit search algorithms were applied.
Results. Forty two sources were classified as planetary transit candidates and up to now 26 cases have been solved. One planet (CoRoT-2b) and one brown-dwarf (CoRoT-3b) have been the subjects of detailed publications.

Key words. techniques: photometric – techniques: radial velocities – techniques: spectroscopic – stars: planetary systems – binaries: eclipsing

1. Introduction

In the present paper we report the initial results of the third pointing of CoRoT (Baglin et al. 2006) that was carried out in the direction towards the constellation of Aquila (LRc01 coordinates: $19^h23^m33.60^s$; $0°27'36''$), in the same spirit as the papers on the

⋆ The CoRoT space mission, launched on December 27 2006, was developed and is operated by CNES, with contributions from Austria, Belgium, Brazil, ESA, Germany and Spain. The first CoRoT data are available to the community from the CoRoT archive: http://idoc-corot.ias.u-psud.fr.

IRa01 by Carpano et al. 2009 and Moutou et al. 2009. We first describe the actual characterization of the field and the methods used in order to detect exoplanetary candidates in the light curves. We then describe the actual follow-up observations carried out and describe the conclusion in each specific case.

In the first selection of candidates in the LRc01 field, 42 candidates were selected for follow-up and characterization. Of these 26 have been settled to date. There are 2 bona fide planets recorded, (Alonso et al. 2008 and Bouchy et al. 2008; Deleuil et al. 2008), the latter of which at 21 Jupiter masses is tentatively classified as a brown dwarf orbiting a solar type star. There are 16 open cases remaining and under further investigation (see below). The remainder of the settled cases are deemed either binaries, grazing binaries or contaminating eclipsing binaries (CEB) where light from an eclipsing binary is blended to the light of a nearby star to produce an event similar to what is expected from a transiting exoplanet in the CoRoT target signal.

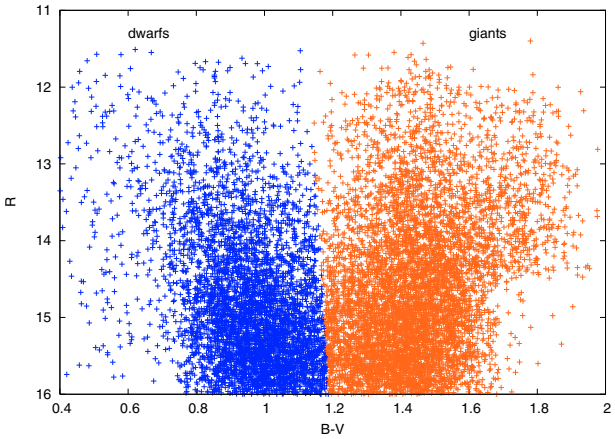

Fig. 1. $B - V$ versus R color−magnitude diagram of the stars in LRc01 field. Dwarf stars are most likely to be found in the left part of the diagram, giants in the right part.

2. Field characterization

The 11 408 targets observed by CoRoT were selected using the information gathered in the database Exo-Dat (Meunier et al. 2007; Deleuil et al. 2009), built with dedicated ground based photometric observations in the visible and near IR bands from 2MASS catalog. CoRoT is a double-purpose mission and the fields observed must achieve a compromise between the requirements of the seismology and the exoplanet science cases. The former requires a small number of bright, well-selected stars and the latter needs a large number of targets due to the relatively low geometric probability (around 5%) of observing a transit, hence fainter stars are observed. Figures 1 and 2 show color-magnitude diagrams of the stars in LRc01 field. Although there is some degeneracy for low-luminosity objects, we can infer from these diagrams that there is a significant fraction of giant stars, up to 58% (see the discussion in Aigrain et al. 2009). Giants are not the best candidates for searching for planets because of their large radius (a Jupiter size planet passing in front of a 6 solar radius star produces a drop in the flux of 0.03% or 0.3 mmag). This reduces the number of optimal targets for the planetary search, although the giants in the field can still produce interesting science thanks to the considerable capabilities of CoRoT (see for example Michel et al. 2008; Gondoin & et al. 2009; Hekker et al. 2009; de Ridder et al. 2009). However, the reduced fraction of dwarf stars has to be taken into account when evaluating the performance of the mission (see Sect. 3).

The precision with which planetary parameters can be measured from photometry relies on the precision for the stellar parameters of the host star. Stellar limb darkening parameters in particular are crucial to this analysis. In theory, these can be obtained from pure photometric analysis, but in practice the degeneracy between the inclination and the limb darkening values and the signal-to-noise ratio required to fully characterize the whole set of parameters make it advisable to fix the limb darkening coefficients (see, for example, Torres et al. 2008). However, this requires a knowledge of the stellar nature which cannot be obtained from CoRoT photometry, requiring input from catalogs or complementary ground-based observations. For CoRoT candidates, we make use of the Exo-Dat database, which includes B, V, R, and I magnitudes for each target, as well as J, H, and K_s from the 2MASS survey, from which temperatures and spectral classes, and thereby limb darkening coefficients, can be estimated.

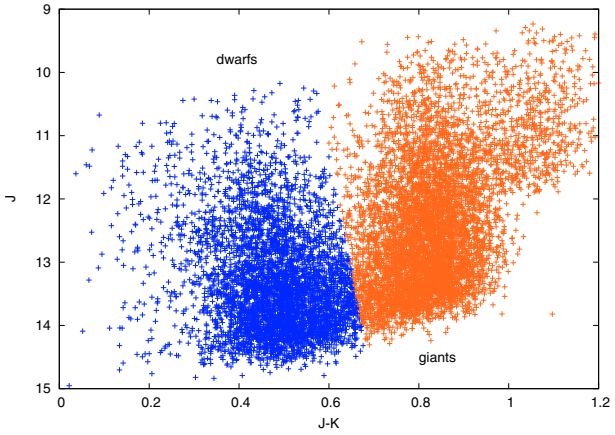

Fig. 2. $J - K$ versus J color−magnitude diagram of the stars in LRc01 field for comparison with Fig. 1. The axes of the figure are fixed for convenience; however, this means that star 101363195, a white dwarf candidate with a $J - K$ of −0.45 and variable with a period of 0.98 days, is not shown.

3. Data reduction

CoRoT samples the stars with a cadence of 512 s (see Surace et al. 2008). However, for a limited number of candidates, a higher cadence of 32 s is available. A bi-prism was installed to disperse the light in the Exoplanet CCD, which helps to distinguish achromatic planetary transits and chromatic stellar variability. For bright stars (32.6% of the targets in the LRc01 field), the flux is measured in three separate channels: *red*, *green*, and *blue*; which have no direct correspondence to any standard photometric band. For the rest of the targets, the flux is measured in a single *white* channel. For a complete description of the observing modes of the satellite, please refer to Boisnard & Auvergne (2006); Barge et al. (2008b), and Auvergne et al. (2009).

Data is furnished to the detection teams at the so-called N2 level (Baudin et al. 2006), the same data made public one year later through the CoRoT archive: `http://idoc-corot.ias.u-psud.fr`. Several treatments have already been applied to eliminate some of the main systematic sources of error (see Drummond et al. 2008; Auvergne et al. 2009). Invalid data points, such as the measurements taken during the passage of the satellite through the South Atlantic Anomaly (SAA) are flagged, this systematic source of noise can easily be avoided. However,

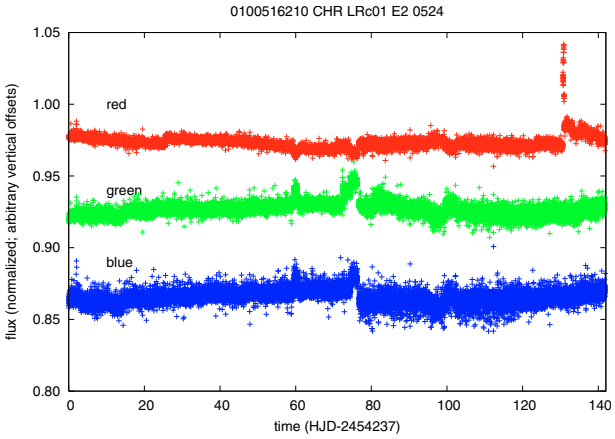

Fig. 3. Example of light curve affected by several instrumental effects. See text for details.

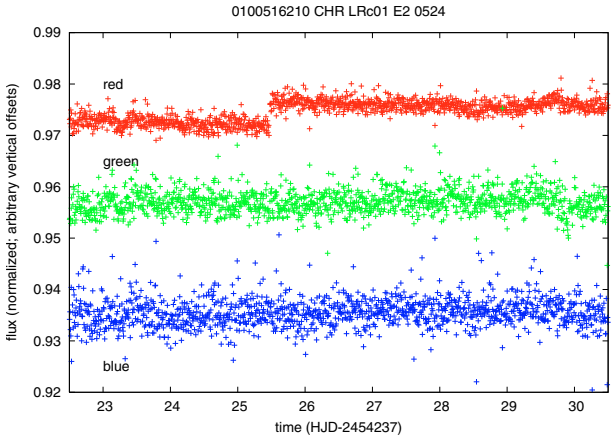

Fig. 4. Detail of the light curve where the red channel is affected by a low-amplitude hot pixel.

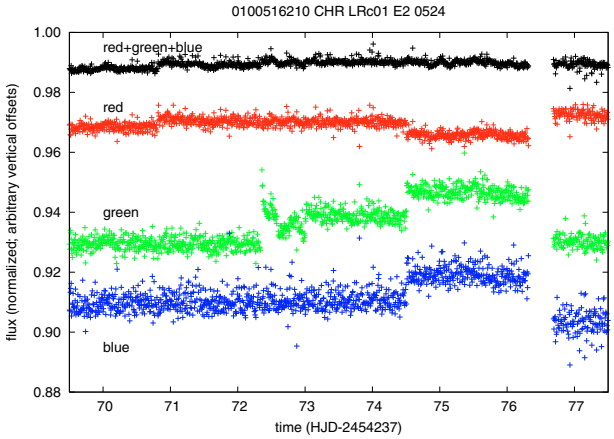

Fig. 5. Detail of the light curve showing different instrumental effects. In $T = 71$ a small-amplitude hot pixel appears in the red channel; in $T = 72.5$ a bigger hot pixel affects the green channel; in $T = 74.5$ there is a change in the flux measured by each channel, but the total flux within the mask remains constant. After the gap in the data in $T = 76.5$ the flux distribution remains stable.

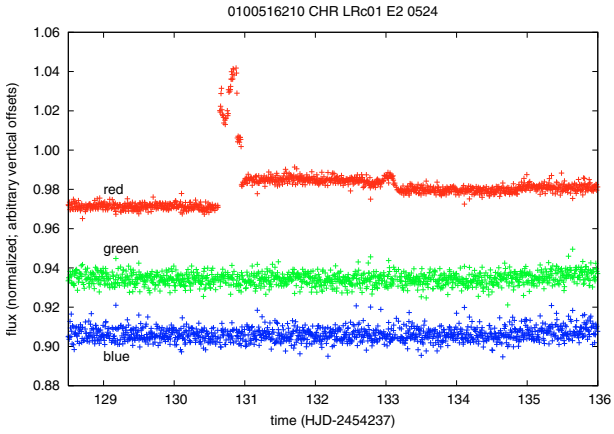

Fig. 6. Detail of the light curve where the red channel is affected by a strong hot pixel, with the change in the relaxation rate around $T = 133$.

other sources of systematic noise remain, such as hot pixels and, in the version 1.2 of the N2 data released in February 2008 (and the one which is used for the results presented in this paper), effects related to the passage of the satellite through the cone of shadow of the Earth illuminated by the Sun. Each detection team uses different techniques to deal with these problems and it is beyond the scope of this work to describe them. However, we show how colored channels are an useful tool for the filtering.

The nature of hot pixels and their incidence in CoRoT's photometry are described in detail in the following papers: Drummond et al. (2008); Pinheiro da Silva et al. (2008), and Auvergne et al. (2009). In Fig. 3[1] we show a typical light curve affected by several instrumental effects that are not filtered by the pipeline. As hot pixels affect only one pixel at a time, it is easy to tell when one of these events occurs by comparing the evolution of the flux in the different channels. Figure 4 shows a detail from one of these events: a moderate intensity hot pixel appears on the red channel and changes the average value of the measured flux, but it does not affect the other channels. Figure 5 shows a detail with a more complicated pattern: in $T = 71$ a small-amplitude hot pixel appears in the red channel; later, in $T = 72.5$ a bigger hot pixel affects the green channel, producing a perturbation that lasts over one day before it is relaxed (although with a different value of the average flux measured); in $T = 74.5$ there is a change in the flux measured by each channel, much like a redistribution of the flux within the mask, because the total flux remains constant. After a gap in the data in $T = 76.5$, the flux redistribution reaches a metastable state that lasts several days. Figure 6 shows the effect of a quite energetic hot pixel in the red channel.

The passage of the satellite through the Earth's umbra is another important source of systematic noise present in version 1.2 of the pipeline (see Auvergne et al. 2009). In future versions of the pipeline, this effect will be flagged and thus be easily avoidable. Nevertheless, the filtering of this phenomenon is relatively straightforward. It is a systematic effect that is present in all light curves, although it has a more severe effect on bright lights curves measured with a small mask (for a description of CoRoT masks, please refer to Llebaria & Guterman 2006) because of border effects (due to jitter, the flux might fall temporally out of the mask). Figure 7 shows a light curve that is strongly affected by this effect, and Fig. 8 shows a detail of the perturbation. The pattern is relatively stable, and the affected points can either be treated as outliers or, as the effect appears always at the same time in the reference frame of the satellite, compiled into a list of affected points that can then be discarded. Recently, Mazeh et al. (2009) have published a paper on the filtering of other systematic effects present in the LRa01 run.

[1] A linear regression was subtracted from the flux in each channel when doing the normalization.

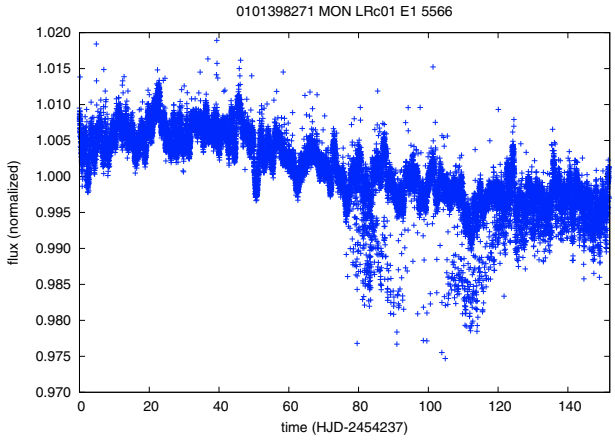

Fig. 7. Light curve affected by systematic sources of noise related to the passage of the satellite through the cone of shadow of the Earth illuminated by the Sun.

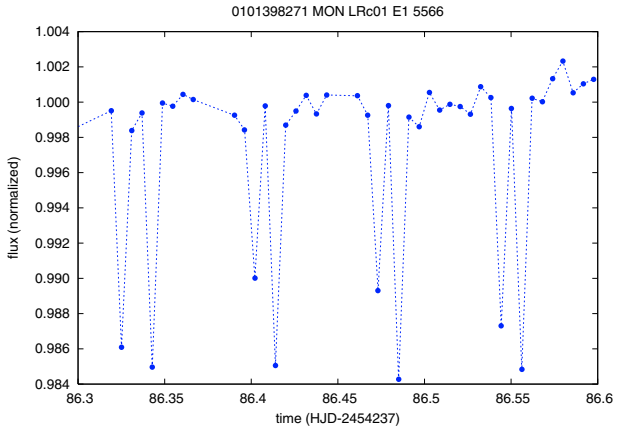

Fig. 8. Detail of the systematic noise related to the passage of the satellite through the Earth's umbra.

This approach appears to reduce the systematic noise in the light curves significantly; although it has not been used in this paper.

The second part of the data processing is the filtering of the stellar activity and the search for transits. Again, each detection team is responsible for constructing and applying its own algorithms. Some of this methods have already been published (Alapini & Aigrain 2008; Bordé et al. 2007; Carpano & Fridlund 2008; Moutou et al. 2005, 2007; Régulo et al. 2007; Renner et al. 2008) so do not need to be described. We do, however, discuss their performances below (also treated in Barge 2009 and Auvergne et al. 2009).

4. Light curve modeling of selected candidates

For the detailed modeling of the transits of planetary candidates, an IDL[2] code with a graphical interface was built[3]. It is based on the transit model by Mandel & Agol (2002) and applies the Amoeba optimization procedure (Press et al. 2002). The code is applied on the filtered and normalized light curves.

[2] IDL is a registered trademark of ITT corporation.

[3] The code can be provided on request to its author: szilard.csizmadia@dlr.de

Table 1. List of the detection teams (institutes and people).

team	participants
DLR	Heike Rauer, Stefan Renner, Anders Erikson
ESTEC	Malcolm Fridlund, Stefania Carpano
U. of Exeter	Suzanne Aigrain, Frédéric Pont, Aude Alapini
IAC	Hans Deeg, José Manuel Almenara, Clara Régulo
IAS	Pascal Bordé, Benjamin Samuel
U. of Köln	Martin Paetzold, Ludmila Carone
LAM	Pierre Barge, Roi Alonso
LUTh	Jean Schneider, Juan Cabrera

For each light curve, we corrected for the impact of possible contaminant sources (the so-called third light) through the following equation:

$$l(\varphi_i) = \frac{1 - \Delta Ł(\varphi_i) + L_3}{1 + L_3} \quad (1)$$

where $l(\varphi_i)$ is the observed, normalized light at phase φ_i, $\Delta Ł(\varphi_i)$ the light loss of the central star due to the transit of a dark object at the same phase expressed in fractions of the unobscured light of the star, and $L_3 = \frac{c}{1-c}$ is the contribution of the contaminant source. The denominator normalizes the light curve at the out-of-eclipse part. Variable c is the contamination factor: the fraction of the total observed light that comes from other, unresolved object(s). We assume that it is constant during the observational interval. This contamination factor – only for the unresolved sources – was obtained from the Exo-Dat database[4].

The parameters that determine the light curve shape are the orbital eccentricity e, the argument of the periastron ω, the epoch and period, two limb-darkening coefficients u_1 and u_2 – we applied the quadratic limb-darkening law, see Claret (1998, 2000)– the planet to stellar radius ratio R_p/R_s, the semi-major axis to stellar radius ratio a/R_s and the inclination i. We assumed that the orbits are circular, $e = \omega = 0$ was set in every case. The limb-darkening coefficients were determined by a bilinear interpolation of the tables in Claret (2000) in the log g-$T_{\rm eff}$ plane (we assumed a solar metallicity for the stars for the sake of simplicity), and the parameters of the central star were taken from the Exo-Dat database. We fixed the epoch and period at their values determined from the light curve itself and calculated the phases. To correct for possible small errors in the phase determination, we introduced a phase-shift similar to the one in the WD-code (Wilson & Devinney 1971), which translates into a constant added to each phase value (found to be very close to zero in every case). Finally, we only had four free parameters: phase-shift, i, R_P/R_s, and a/R_s. We tried several different starting points and each the four parameters were fitted simultaneously by the Amoeba-procedure mentioned above.

The results of the light curve modeling of the candidate E2_1145 is reported in Sect. 6.3.1.

5. Results

Detection teams, shown in Table 1, were assigned the task of detrending and analyzing the data searching for transits. The data was delivered to the teams on 16 February 2008, one year before it was made public. However, this was not the first time

[4] this value is present in the header of the fits file of every light curve provided by the CoRoT archive.

that data from the LRc01 had been analyzed. The alarm mode regularly analyzes CoRoT N0 data (raw data from the satellite) during the space observations to decide which targets have to be oversampled (observed with the 32 s cadence) and to allow an early detection of planetary transits, which can be followed-up immediately. Such is the case of all the planets detected so far by CoRoT.

Each detection team applied different techniques to detrending the light curves and searching for transits (see, for example, Alapini & Aigrain 2008; Bordé et al. 2007; Carpano & Fridlund 2008; Moutou et al. 2005, 2007; Régulo et al. 2007; Renner et al. 2008). Then all the candidates found by each team were discussed in regular telephonic teleconferences. Most of them were found by several teams (if not all), but some cases were only found by a single team. A certain number were just false alarms, but sometimes real candidates were discovered that felt just under the detection threshold fixed by the rest of the teams. As pointed out by Moutou et al. (2005), one of the main advantages of having different teams using different techniques is that false alarms depend on the method. Candidates were sorted in a priority list whose hierarchy depended on the quality and the planetary likelihood of the signal: the shape of the transit, the possible existence of out-of-transit variations, the possibility of discarding a secondary eclipse (which will be a clear hint of a binary nature of the candidate), the color of the transit, the depth and the duration of the transit (Seager & Mallén-Ornelas 2003), and the star's spectral type. Although, before discarding for good any candidate we waited for the spectroscopic confirmation of the stellar nature, as the photometric characterization of Exo-Dat might not be 100% reliable. The aim is to discard as many as possible of the scenarios mimicking planetary transits from photometry (see Pont et al. 2005). The hierarchy established several categories: 1 (first class candidates that showed no problems); 2 and 3 (candidates that showed some problems in any of the properties needed to assess their planetary nature, although they could not be discarded as binaries just from the photometric analysis of the light curve furnished by CoRoT); and finally some problematic candidates were classified as category 4, where the analysis on these candidates was pursued, although they were generally not followed-up.

The ordered list of candidates was passed to the follow-up team, which decided its own hierarchy as function of the input from the detection teams, the magnitude of the target, and the disponibility of the observational facilities.

The detection team provided a list with 7 priority 1 candidates. Three of them had been previously reported by the alarm mode (including the planet CoRoT-2b and the brown dwarf CoRoT-3b); 6 of the 7 were solved by the follow-up, characterized as one planet (CoRoT-2b), one brown dwarf (CoRoT-3b), two blends, one contaminating eclipsing binary (CEB), and one SB1; one candidate is still being observed. There were 8 priority 2 candidates: 5 solved by the follow-up: two CEBs, one SB1 and two SB2; 3 candidates are still being observed. Fifteen candidates were classified as priority 3: 6 have been solved: one blend, two CEBs, three SB1, and 9 candidates have not been solved so far. Finally, 13 candidates were classified as priority 4.

Table 4 presents those planetary candidates that have not yet been resolved by follow-up observations. Table 5 shows the candidates whose nature has been established from spectroscopic or photometric ground-based observations. Finally, Table 6 is a list of the 158 eclipsing binaries characterized by the detection teams. The scientific task of the detection teams is to provide a characterized set of planetary transiting candidates; although as a natural by-product they build a list of identified eclipsing binaries which is provided here. Some of the binaries (such as E1_1922, E2_0170, E2_1450, E2_3052, E1_1262, and E2_0169) have already been observed by Karoff et al. (2007) within the Berlin Exoplanet Search Telescope (BEST) survey of variable stars in the CoRoT fields. Among the binaries in the list, the following are clearly eccentric: E1_1273, E1_1352, E1_1422, E1_2978, E1_3418, E1_3671, E1_4583, E1_5097, E1_5173, E2_0258, E2_0667, E2_1661, E2_1954, E2_2257, E2_2631, E2_2871, E2_3956, E2_3995, E2_5245. And some show pulsations (like E2_0844). Obviously, also many variable stars were found, but the task of classifying and characterizing the variables is done by another team (see Debosscher et al. 2009). Among the single eclipse events, there is one curiosity, E2_0379, which shows a primary eclipse 13% deep; 21.1 days later it shows a secondary (0.21% deep) and nothing else during the next 120 days of observation. The simplest explanation is a long-period eccentric binary. Observations taken with IDS at the Isaac Newton Telescope on the Canary Islands reveal that the spectral type of the main star is B8V.

6. Detailed follow-up of candidates

6.1. Ground-based observations

The CoRoT observations allow us to detect new classes of transiting exoplanets, viz. very small planets (Léger et al. 2009), brown dwarfs (Deleuil et al. 2008), and objects with very long and short periods. A prerequisite for this is, however, a well-developed and organized ground-based follow-up program. The CoRoT point-spread function (PSF) covers about 50 pixels (depending on magnitude and color, see Auvergne et al. 2009) and background objects can contribute to the CoRoT light curve, particularly contaminating eclipsing binaries (CEB). They are relatively easily detected, however, by carrying out ground-based photometry during and out of eclipse, since an object some arcseconds distant from the target star will only contribute a small part to the light curve, and therefore needs to have a large-amplitude eclipse. This photometry goes under the designation ON-OFF photometry, and the major problem is having a suitable telescope ready at the right time for the ON observation. We refer to Deeg et al. (2009) for details.

Grazing binaries, intrinsic stellar pulsations, and stellar activity are other "contaminants" where the CoRoT light curve can mimic a transiting planet, particularly one of small amplitude. Both high spectral resolution spectroscopy and high-precision radial velocity spectroscopy are necessary, the latter also for determining the mass and comparing and refining the orbital parameters derived from the light curve. The contaminant candidates identified through this procedure are SB1, SB2, blends, and CEB's.

In the case of both photometry and spectroscopy, CoRoT requires large resources and use both "normal" observations acquired through the time allocation process, particularly at the European Southern Observatory (ESO), the Observatoire d'Haute Provence (OHP), the Instituto Astrofísica de Canarias (IAC), and McDonald observatory. In this context dedicated time also brought into the CoRoT project through partners and collaborations are utilized, such as the Israeli Wise observatory, the HARPS and EULER guaranteed time of the Observatoire de Geneva, the low-resolution spectrograph of the Türinger Landessternwarte Tautenburg (TLS), and ESAs Optical Ground Station (OGS) facility in Tenerife.

6.1.1. False positives

Contaminating eclipsing binary (CEB). This is the case when a background object that falls within the PSF of CoRoT happens to be an eclipsing binary itself. There are cases where the contaminant was brighter than the target, and without knowing spectral types, we do not really know (or care) if contaminants are foreground or background. It will then affect the CoRoT light curve, contributing some fraction of a percent to the light curve and thus be taken for a variation in the target star itself. CEBs can be identified if the CoRoT light curve happens to be a chromatic one and the variation with color is wrong for the target, as was the case in the first identified low-amplitude eclipse signal found in one of the first observations reduced. The variation in the white light curve was just 0.002, while it was several percent in the blue light curve, thus identifying the variation as belonging to a fainter, eclipsing binary in the blue part of the background. Lacking chromatic light curves, or in complicated cases, ON-OFF photometry is carried out as described below.

SB1 (a single-lined spectroscopic binary, where only one component is visible), SB2 (a double-lined spectroscopic binary, where both components are visible), and blends (unresolved triple systems) cannot be solved by photometric observations, because the variability occurs in the target. To confirm the nature of the system, we need to know the mass of the object that is producing the periodic dips in the light curve. SB2 can be easily discarded with a few observations, but other configurations, such as multiple stellar systems, might require more effort.

6.1.2. Photometry

The photometry to be carried out can be broadly divided into two classes. First, calibrated color-photometry of potential CoRoT target fields was performed before the CoRoT mission was launched, in order to select the target fine pointings and to characterize the stars in the finally selected fields. This gave rise to the Exo-Cat photometric catalog within the Exo-Dat information system for CoRoT's exoplanetary program. It was built using mainly the Isaac Newton 2.5 m Telescope (INT) at the Roque de los Muchachos observatory in La Palma, Spain and its WFC camera. This camera has a field of view of 34.′5 and a pixel scale of 0.″33. The second instrument used for target selection was the Megacam on the 3.6 m Canada France Hawaii Telescope (CFHT) on Manua Kea, Hawii. This camera has a 60′ by 60′ field of view with 0.″187 pixel resolution.

A photometric follow-up program of individual candidates was initiated to verify that eclipses detected by CoRoT are on the presumed target. It mainly employs ON-OFF photometry, where candidates are observed briefly during a transit, and again off-transit, and their brightness and that of any nearby star is compared. This program and its techniques are described in more detail in Deeg et al. (2009). For the period in question, mainly three instruments have been used. The first is EulerCam on the 1.2 m Leonard Euler telescope at La Silla, Chile. The second is the Wise observatory in Israel with its 1m telescope, using the Princeton Instruments (PI) camera. Finally, the third telescope is the 80cm telescope of the Instituto de Astrofísica de Canarias (IAC) at the Observatorio del Teide in Tenerife, Spain. A database of ephemeris is maintained at IAC.

6.1.3. Spectroscopy

The spectroscopy is also broadly divided into two classes. First there is the verification of the planet through radial velocity observations. Ideally, a chain of observations are carried out beginning with the identification of SB's using the CORALIE spectrograph on the 1.2 m Leonard Euler telescope at La Silla and the Sandiford cassegrain echelle spectrograph at McDonald Observatory. After passing this test, the planetary candidate star is observed with SOPHIE, a high-resolution spectrograph on the 1.93 m telescope at the Observatoire de Haute Provence (OHP), which in high-resolution mode provides a resolution of 76 500 over a wavelength range of 3872−6943 Å. With various cross-correlation techniques, this allows radial velocities down to maybe 3−4 m/s for the brighter stars in the sample. The final radial velocity stage uses the HARPS spectrograph, which is fiber-fed by the 3.6 m reflector at La Silla Chile. HARPS provides a resolution of 115 000 over a wavelength range of 3780−6910 Å. For the faint stars in the CoRoT sample, the signal-to-noise in a typical observation is ∼20. Nevertheless, a precision of 2−3 m/s can be achieved with a number of well sampled observations, with the best so far for a CoRoT star being 1.2 m/s after ∼120 individual observations (Queloz, in preparation).

The second spectroscopic mode is for stellar characterization. For some of the CoRoT candidates, low-resolution spectroscopy ($R \approx 1400-2100$) was performed using the Nasmyth spectrograph mounted at the 2-m-Alfred Jensch telescope of the Thüringer Landessternwarte Tautenburg (TLS). These observations are useful for assessing the nature of some interesting candidates (Gandolfi et al. 2008), and it eventually triggers further radial velocity follow-ups, as well as identifying and ruling out hot objects (B and early A stars) and giant stars. On the other hand, a high-resolution spectrum is required for determining the stellar parameters, and large telescopes are required, since the majority of the CoRoT targets are faint. For the LRc01 region, essentially all spectra have been obtained using the 8 m class VLT's of ESO in combination with the UVES and GIRAFFE high-resolution spectrographs – occasionally with the FLAMES multi-fiber positioner as a front-end.

6.2. Planets

6.2.1. LRc01 E1 0523 – CHR – 0101368192

This object, designated CoRoT-3b, was discovered in the alarm mode after 67 days, whereupon the 512 s integration time was changed for 32 s cadence. The follow-up process is described in Deleuil et al. (2008). Originally classed in the Exo-Dat database as a G2V star, the host was found to have a $T_{\rm eff}$ of 6740 ± 140 K, after the follow-up spectroscopy carried out with the VLT/UVES combination. With a value of $\log g$ of ∼4.2, it is thus more representative of an early F-type star (F3V, Deleuil et al. 2008). The planetary mass turns out to be 21.66 $M_{\rm Jup}$, and the radius is 1.01 $R_{\rm Jup}$. Deleuil et al. (2008) therefore conclude that this is the first secure inhabitant of the so-called "brown dwarf desert". Maybe more important, the accurately determined radius confirms model predictions of what this parameter is expected to be in an evolved brown dwarf. Burrows et al. (2001) present model calculations, and demonstrate the radius of brown dwarf type objects to be 1 $R_{\rm Jup}$ after 300 Myr and 1 Gyr for intermediate and low-mass objects, respectively. As pointed out by Burgasser et al. (2009), the surface gravity of a >100 million year old brown dwarf will be similar to the values derived for this object.

6.2.2. LRc01 E2 0192 – CHR – 0101206560

This object, designated CoRoT-2b (Alonso et al. 2008; Bouchy et al. 2008), was also discovered in alarm mode. The star is

Table 2. Parameters for the fits of the planetary candidate LRc01_E2_1145 shown in Fig. 9 (see explanation of the parameters in Sect. 4).

parameter	E2_1145
Period (days; fixed)	6.212 242 ± 0.000 013
R_p/R_s	0.081 6 ± 0.003 2
a/R_s	14.3 ± 1.4
i (deg)	87.1 ± 0.6
e (fixed)	0
u_1 (fixed)	0.556
u_2 (fixed)	0.212
third light (fixed)	0.0

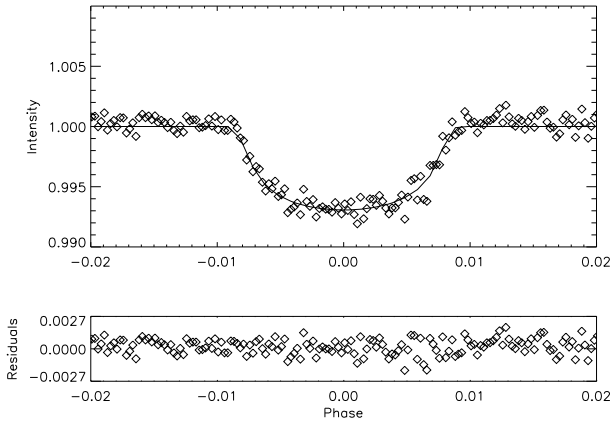

Fig. 9. Normalized, binned, and phase-folded light curve of the candidate LRc01_E2_1145. The transit depth is compatible with a 0.7 Jupiter radii object.

visibly highly active with a significant spot activity (Alonso et al. 2008; Lanza et al. 2009). The star is of solar type, with $T_{\rm eff}$ of 5625 ± 120 K, a value of $\log g$ of 4.3 ± 0.2, a solar metallicity, a radius of $0.92 \pm 0.02\,R_\odot$, and a $v \sin i$ of about 12 km s^{-1} (Alonso et al. 2008; Bouchy et al. 2008). The high value of $v \sin i$, taken with the value of i derived from the light curve parameters as well as the rotational period derived from the light curve are all consistent with the radius derived from the stellar modeling and all aspects point towards a very young object with an age below 0.5 Gy (Bouchy et al. 2008).

6.3. Suspected planets or unsettled cases

This section includes objects that are still being followed-up because their nature as a planetary transit has not been disproved. We also include targets, where there are indications of a non-binary nature, which has downgraded the priority, and lack of resources have caused them not to be followed-up. The possibility remains of the eclipses being caused by an exoplanetary object, but we stress that these targets are unsettled.

6.3.1. LRc01 E2 1145 – CHR – 0101086161

Discovered in alarm mode, the follow-up on this candidate has not been finished, but the first radial velocity measurements are compatible with a planetary mass companion to the star, although the possibility of a blend scenario has not been ruled out completely. UVES observations indicate a $T_{\rm eff}$ of 5350 K, a $\log g$ of 4.4, and the spectral type of the star is thus K0V. Then assuming a radius of 0.85 $R_\odot$, the potential planet has a size of 0.7 $R_{\rm Jup}$ (see Table 2 and Fig. 9).

6.3.2. LRc01 E2 5801 – MON – 0100905839

A difficult light curve with many hot pixels and probably some damaged pixels within the readout window. It is a monochromatic light curve, and therefore difficult to filter. Nevertheless, the suspected planetary signal appears clear. The period is relatively long, 15.7 d, the depth of the eclipse is 0.70%, and the eclipse lasts for 3.9 h. The true nature of this candidate has not been definitively established yet because the follow-up is not complete. Anyway, on the basis of the spectral analysis performed on a low S/N UVES spectrum, the object should be a K0 dwarf-star.

We do not present a model of the light-curve as we did with the previous candidate because of the difficulty of assessing the reliability of the fitted parameters. The model of a transiting planet is understood, but the difficulty with this particular light curve is the low signal-to-noise ratio and the impact of the instrumental sources of noise and the hot-pixels. The more aggressive the filtering of those systematics, the more affected the shape of the transit, and it is difficult to calculate how much the parameters obtained from the fit depend on the filtering used. However, we are sure about the periodic signal because we can observe 9 full consecutive transits, and about the size that we infer for the candidate, which is below 1 Jupiter radius if the star is a dwarf and the transit is on target.

6.3.3. LRc01 E2 1802 – MON – 0100725706

This candidate was discovered in alarm mode with a period of 13.239993d and a depth of 1.18%. The star was classified as K5V (Exo-Dat), and m_V = 15.2. HARPS observations are not conclusive due to Moon contamination, although the residual variations are compatible with photometric ephemeris and a substellar secondary mass.

6.3.4. LRc01 E1 1929 – CHR – 0101206989

This object is classified as K5V in the Exo-Dat database and has a m_V = 15.0. The period is only 0.577 d, the depth 0.3%, and the duration 1.3 h. Unfortunately, the signal is only seen in the blue light curve. Radial velocity observations with SOPHIE proved inconclusive (the limit in the variation is as low as 15 m/s); photometry with IAC80 demonstrated that the closest fainter stars that could mimic the transit are not variable. On the basis of low-resolution spectroscopy carried out at TLS, the spectral type of the star is most likely K0III/IV. The follow-up has recently been stopped on this target because some hints of a secondary eclipse had been found in the CoRoT light curve.

6.3.5. LRc01 E2 3345 – MON – 0101332685

This object has a depth of 3.6%, and a period of 13.099d. Because the star is a K5V of m_V = 15.8, it was observed with HARPS 4 times. The diluted amplitude of the blend is about 60 m/s, whereas individual error on the measurements range from 22 to 66 m/s, so the blend variation is hardly significant.

6.3.6. LRc01 E1 4780 – MON – 0101186644

An m_V = 16.0 K0V (Exo-Dat) star with a relatively deep (0.86%) eclipse with a period of 20.684d. HARPS observations are not conclusive due to Moon contamination. At twice the period determined from the photometry, the radial velocity measurements result in a signal with a few km/s amplitude, but this possibility should be confirmed with new observations not affected by Moon contamination.

6.3.7. LRc01 E1 0715 – CHR – 0101157411

This is a single transit that is 9 h long with a depth of 0.6%. The spectral classification in the Exo-Dat database is G2IV, and its visual magnitude is m_V= 13.6. Two observations with SOPHIE were carried out with a separation of 60 days. No variation was detected and a case of SB1 appears to be excluded. A UVES spectrum was obtained and the following preliminary parameters are derived from this spectrum: the star is roughly solar type, with dwarf characteristics (F8/9 V). It has, however, a high value of $v \sin i$, ∼14 km s^{-1}, which makes the interpretation difficult.

6.3.8. LRc01 E2 4295 – MON – 0101123916

This candidate has a low priority because it is faint, and there are marginal indications of a secondary in the light curve. The target star has an m_V = 16.5, and a spectral type according to Exo-Dat of M0V. With a period of 1.13828d and a depth of the eclipse of 0.28% (duration 2.9 h), it could be a similar case to the CoRoT-7b super Earth (Léger et al. 2009). Photometry is planned for this source in 2009 to discard a CEB scenario.

6.3.9. LRc01 E1 1632 – CHR – 0101424939

This source was identified as a binary by two teams and as a low priority planetary candidate by one team. A reanalysis seems to identify a secondary in the light curve, so the object has been placed on hold. The primary is identified as a K0IV from photometry (Exo-Dat) and has a m_V = 14.9.

6.3.10. LRc01 E2 4390 – MON – 0100768215

This object has a low priority because two of the detection teams find hints of a secondary eclipse. Nevertheless, photometry carried out at the CFHT and at IAC80 demonstrates that the eclipse is on target. The star is identified as a M0V, with a m_V = 16.5. The period is 2.94 d, the depth 0.3% and the duration 4.1 h. The nature of this object is still unknown, but its faint magnitude makes it a very difficult target for spectroscopic follow-up observations.

6.3.11. LRc01 E2 0934 – CHR – 0100887662

A single transit of 8.6h duration and 2.28% depth around a G8V star and with m_V = 14.1 from Exo-Dat. It has not been followed-up so far.

6.3.12. LRc01 E1 0673 – CHR – 0100980128

A candidate with a period of 6.00234d and a depth of 0.1%. The Exo-Dat catalog reports a G5IV star with m_V = 13.5. On the basis of a low-resolution spectrum acquired at TLS, we estimated that the candidate might be an F8/G0 dwarf star. Radial velocity follow-up is currently going on for this target.

6.3.13. LRc01 E1 2761 – MON – 0101439653

This is a candidate with a period of 17.49731d and a depth of 4.11% in a K0V (Exo-Dat) star of m_V = 15.2. It has not been followed up.

6.3.14. LRc01 E1 1791 – CHR – 0101115531

This is a candidate with low priority because of the shape of the light curve. There is an out of transit variation, and the signal is only found in the red channel, facts which point to a CEB scenario. It has a period of 0.520959d and a depth of 0.18% in a K5V (Exo-Dat) star of m_V = 14.9. It has not been followed up.

6.3.15. LRc01 E2 4241 – MON – 0100654833

This object was only detected by one team and it was kept as priority 3 because the possibility of being a false alarm was not ruled out. Exo-Dat gave K5V and m_V = 15.9. Period is 0.53108d, depth 0.11%, and duration is 2.3 h. Observations with FLAMES indicate an SB1 but is uncertain. Photometry is to be carried out before settling this case definitively.

6.3.16. LRc01 E1 2278 – MON – 0101614469

This is a shallow candidate with a long transit, it was flagged as low priority. Exo-Dat gave K5V and m_V = 15.2. Low-resolution spectroscopy performed at TLS suggested that the candidate is a G8/K0 giant star. Three HARPS measurements are not conclusive: they are not in phase with CoRoT ephemeris, but individual errors range from 20 to 50 m/s.

6.4. Settled cases - non-planetary objects

6.4.1. LRc01 E2 5365 – MON - 0100567226

This candidate shows some variability at the 1% level, which is not correlated with the transit detection. Two observations with the UVES+FLAMES combination demonstrate radial velocities of −9.33 km s^{-1} and −4.56 km s^{-1} at CoRoT phases of 0.62 and 0.87, respectively. The object is thus classified as type SB1 and further analysis is left for a later time.

6.4.2. LRc01 E2 3681 – MON – 0110604224

This candidate is similar to the previous one, a short period (3.45075d) and a slightly long eclipse (2.8 h) for the period. It is a faint star m_V 15.7, with a shallow depth of the eclipse (0,15%). Although the Exo-Dat database gave G2IV as the spectral type, it was classified in priority 1. Photometry with EULER during eclipse saw no indication of variation on the target, but a 15% eclipse on a 1.3 times fainter star, 12″distant was detected and later confirmed with the IAC80 telescope. This is thus another case of a CEB.

6.4.3. LRc01 E2 0305 – CHR – 0101351899

This is a very interesting target that shows pulsations with a period of 0.168 days. It shows a clear sign of a transit with a period of 10.99 days and depth around 1%. That the light curve is

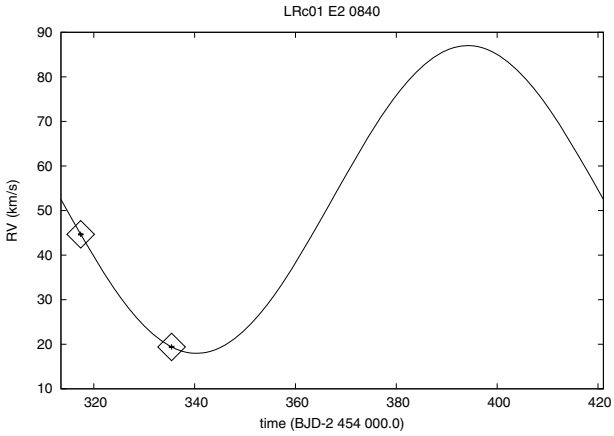

Fig. 10. Radial velocity curve and rough adjustement of an orbital solution with a period of 107.5878 days.

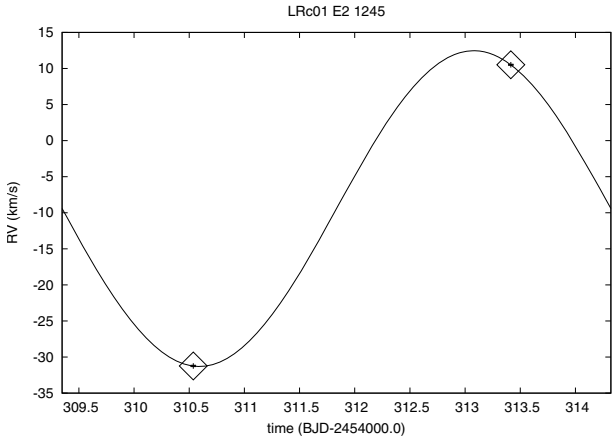

Fig. 11. Radial velocity curve and rough adjustement of an orbital solution with a period of 4.974 days.

chromatic allowed extensive analysis and it was ranked as a binary by 2 detection teams because of the depth differences between different channels (around 1% in red and green but 0.5% in the blue channel). The possibility existed that a background contaminant in the blue channel could account for those depth differences and the candidate finally obtained priority 2. The Exo-Dat database classified it as G2V and m_V = 13. SOPHIE observations detected a wide single peak, and the second measurement showed a change in radial velocity of 58 km s^{-1}, thus, indicating an SB1 type binary, but at twice the period detected by the photometry: 21.97 days.

6.4.4. LRc01 E1 3129 – MON – 0101436549

This is a G2V star (Exo-Dat) of m_V = 15.2, whose light curve looked promising. Low-resolution spectroscopy at TLS indicates a early F star. Photometry with IAC80 showed the eclipse to be on a neighboring, 3.5 mag fainter star ∼12″ distant. The eclipse depth is 0.7 mag. It is thus a CEB

6.4.5. LRc01 E1 0769 – CHR – 0101068850

Another single-transit, 7 h long and 4% deep on a star classifed as K5V by Exo-Dat and with a magnitude of m_V 14.0. It was observed twice with SOPHIE and it seems to be an SB2 type binary. The observations are compatible with a period of the binary in the range of 100 to 300 days.

6.4.6. LRc01 E2 4006 – MON – 0100589010

This is another K5V star (from Exo-Dat) and a rather faint at m_V = 15.9 one. The period is again quite short (0.781d) and it has a depth of 0.14%. Some HARPS observations were carried out, but with no significant result, partly because the spectra had very low signal-to-noise ratio. Finally, photometry at Wise observatory demonstrated that the eclipse was on a background star.

6.4.7. LRc01 E2 3895 – MON – 0100609705

This is a very shallow transit (0.09%) with a period of 3.30382d on a m_V = 15.8 G8IV star (from Exo-Dat). It was immediately identified as a CEB by observations with EULER and IAC80.

6.4.8. LRc01 E1 1253 – CHR – 0101653417

This is a brighter object with a 0.15% eclipse on a K5V m_V =14.6 star (from Exo-Dat) and with a period of 5.7799d. Three observations with SOPHIE demonstrated a blend.

6.4.9. LRc01 E1 1090 – CHR – 0100982006

This target was discovered in alarm mode, and settled with the first spectra. It is a clear SB1.

6.4.10. LRc01 E1 2936 – MON – 0101708400

This is a G2V (Exo-Dat) of m_V = 15.2, 4.2202209d period and a depth of 0.85%. Observations with GIRAFFE+FLAMES indicate an SB1 binary.

6.4.11. LRc01 E1 2837 – CHR – 0101482707

This object demonstrates the difficulties with programs that depend on large statistical samples, since the spectral type in Exo-Dat came out as a G5 super giant of m_V = 13.4. The period was found as 39.8883d and the depth of 1.31% was right for this period if the star was a dwarf. A spectrum was clearly indicated and was obtained by SOPHIE. Unfortunately, the star was shown to be a binary of type SB2.

6.4.12. LRc01 E2 0840 – CHR – 0101031117

This is an interesting case found in alarm mode. The period is 53.8141d, the depth is 0.60%, and the duration 3.8 h in a K0V (ExoDaT) of m_V = 13.9. The follow-up classifies it as SB1 but with twice the period formerly proposed by the detection team (see Fig. 10).

6.4.13. LRc01 E2 1245 – CHR – 0100773735

This candidate was discovered by alarm mode, and Exo-Dat classifyed it as G8V of m_V = 14.0. The period is 4.974d, depth = 0.66%, and the duration is somewhat long. From the SOPHIE spectrum it is not possible to clarify whether we have a multiple component binary (SB2 or SB3) or a single component (SB1). In any case, this is a spectroscopic binary and one can clearly measure the movement of one of the components between the extreme phases of the orbit detected by CoRoT (see Fig. 11).

6.4.14. LRc01 E1 5626 – MON – 0101259269

This candidate, K5V (Exo-Dat) and m_V = 15.9, was relatively quickly found to have a secondary eclipse and was downgraded to a binary. No follow-up was carried out.

6.4.15. LRc01 E1 1845 – MON – 0101218359

This candidate, K5V (Exo-Dat) and m_V = 15.2 was also found to have a secondary eclipse so was downgraded to a binary. No follow-up was carried out.

6.4.16. LRc01 E2 2533 – MON – 0100468104

This candidate, K0IV (Exo-Dat) and m_V = 15.2 was found to have a secondary eclipse so was downgraded to a binary. No follow-up was carried out.

6.4.17. LRc01 E2 5414 – MON – 0100834293

This candidate was discovered in alarm mode and with parameters of G0IV and m_V =16.4 from Exo-Dat. ON-OFF photometry was carried out with the IAC80 and the eclipse was found to be on target. A large secondary at phase 0.41 was in the meantime discovered in the CoRoT light curve (period 11.30d) and it was re-classified as an eccentric binary.

6.4.18. LRc01 E1 5745 – MON – 0101026464

This candidate,G2V (Exo-Dat) and m_V = 16.3 was found to have a secondary eclipse and downgraded to a binary. No follow-up was carried out.

6.4.19. LRc01 E1 3425 – CHR – 0101434308

This candidate,G2V (Exo-Dat) and m_V = 14.8 was found to have a secondary eclipse and downgraded to a binary. The transit is seen mainly in the blue channel, where it is 2.7% deep. No follow-up was carried out.

6.4.20. LRc01 E2 3257 – MON – 0101106246

Another alarm mode candidate. Spectral type M2V and m_V = 16.2 (from Exo-Dat), with a period of 11.31662d and a depth of 0.33% it appeared promising, but ON-OFF photometry with EULER and IAC80 found a nearby eclipsing binary contaminating the PSF of the target star.

6.4.21. LRc01 E1 2376 – CHR – 0101095286

Exo-Dat classified this candidate as K5III and m_V = 13.6. The follow-up demonstrated the binary nature of this object through ON-OFF photometry at IAC80.

6.4.22. LRc01 E1 4959 – MON – 0101175376

This case is similar to the previous case (LRc01 E1 2376).

6.4.23. LRc01 E1 2140 – MON – 0101055792

This object was found by one of the CoRoT detection teams. Since the eclipse signature was deemed to be slightly too long for the period (i.e. 2.0 h and 1.9384d, respectively), low priority was originally assigned to this star; however, the star was classified as a K5V in the Exo-Dat database (m_V = 15.1). Furthermore, low-resolution spectra taken at TLS indicated a late G star with a luminosity class compatible with a dwarf or subgiant. On the basis of these results, the radius of the star might be as small as 0.76 $R_\odot$. The shallow eclipse (0.13%) then indicated that the planetary candidate radius could be as small as 2.8 $R_\oplus$. The target was therefore upgraded to priority 1 in spite of the faint magnitude and transit duration, and further follow-up observations were started. Ground-based observations at IAC80 confirmed that the transit was on target. The object was then observed three times with SOPHIE and scheduled for HARPS follow-up observations when a blend was suspected. Finally, from the HARPS run, the candidate turned out to be a blend with a spatially unresolved eclipsing binary.

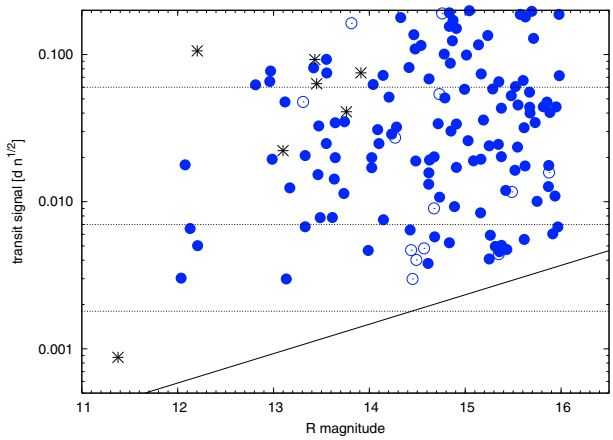

Fig. 12. Transit signal vs. R magnitude for the objects described in this paper. Filled circles are identified objects (Tables 5 and 6) and open circles are for objects in ongoing follow-up (Table 4). The asterisks represent the position of the six planets, and the brown dwarf discovered by CoRoT (CoRoT-7b is in the *bottom left corner*). The horizontal dashed lines represent (*from top to bottom*) the expected signal produced by a Jupiter-size planet, a Neptune-size planet, and a 2 Earth-radii planet, respectively.

6.4.24. LRc01 E1 4863 – CHR – 0101675703

This was a shallow candidate on a K5V of m_V = 16.0 (from Exo-Dat). It was flagged as low priority because one team classified it as a binary since the eclipse was deemed too long (2.4 h) for the period (1.79308d). HARPS measurements finally concluded that the candidate is a blended eclipsing binary.

7. Detection statistics

To measure the performance of a transit survey, it is very useful to follow the approach described by Pont et al. (2006): calculating the noise at the time scales of the transit. This work is described in Aigrain et al. (2009) as it relates to the first three long runs observed by CoRoT. The latter paper conclude that *the photometric performance on transit timescales is close to the pre-launch specification*, and no significant differences between the three fields are found, apart from a slight *gradual degradation of the photometric performance over time, which may be associated with the increase in incidence of hot pixel events*. In LRc01, the photometric performance of CoRoT is 7.1×10^{-4} at R = 15 at the sampling of 512 s, conforming to pre-launch specifications.

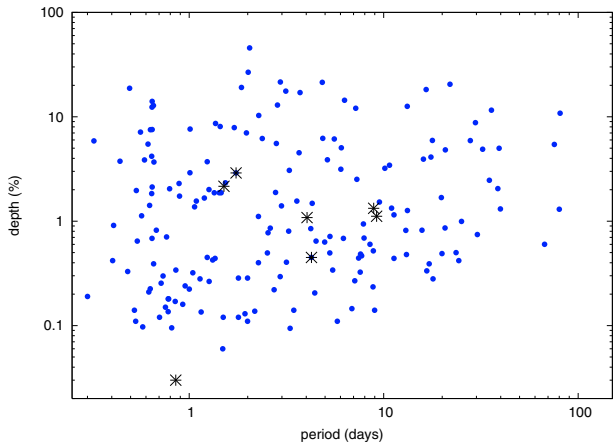

Fig. 13. Depth of the candidates versus their period. The points are for the candidates found in the LRc01 run, and the asterisks are the planetary like objects found by CoRoT. See the interpretation in the text.

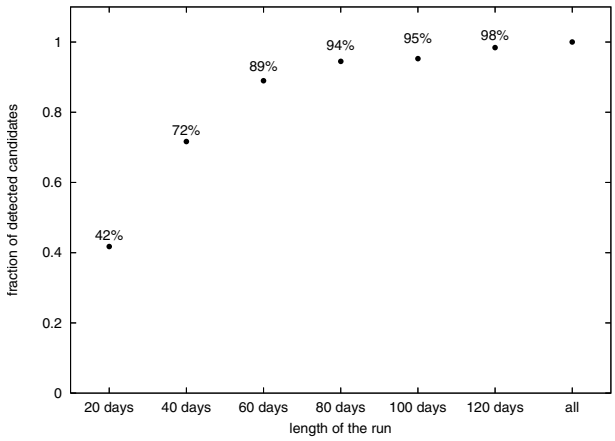

Fig. 14. Evolution of the fraction of candidates detected in a whole run as a function of the length of the run.

Figure 12 represents the transit signal (the product of the relative depth of the transit and the square root of the number of points in the transit) versus the R magnitude. It shows the position of the solved candidates in the LRc01 (Tables 5 and 6) and the ongoing candidates (Table 4), as well as the position of the 6+1 planetary-like objects discovered by CoRoT (6 planets: CoRoT-1b: Barge et al. 2008a; CoRoT-2b: Alonso et al. 2008 and Bouchy et al. 2008; CoRoT-4b: Aigrain et al. 2008 and Moutou et al. 2008; CoRoT-5b: Rauer et al. 2009; CoRoT-6b: Fridlund, in preparation; CoRoT-7b: Léger et al. 2009; and one brown dwarf: CoRoT-3b: Deleuil et al. 2008). In this context, the word "candidate" is used in a broad sense: any target that shows a periodic behavior that can be either a planetary transit or, more likely, an eclipsing binary. The effective detection threshold appears to lie slightly higher than the photon noise limit and a cutoff seems to exist in that no candidate is detected below a transit signal of 0.003. However, it has to be taken into account that the 0.003 level is only reached for magnitudes brighter than 14. Only 24% of LRc01 candidates are in this range of magnitude, and only 7% in the range brighter than 13. Probably few of them are dwarf stars. CoRoT-7b clearly stands below the 0.003 threshold, but it was discovered in the LRa01, which had a different stellar population. Probably, the 0.003 threshold (thought to be 0.009 for the IRa01) stems from low number statistics: the short amount of suitable targets in this magnitude range. Taking Fig. 12 into account, the diagrams published by Carpano et al. (2009) and Moutou et al. (2009), as well as the noise studies by Aigrain et al. (2009), it seems plausible to state that CoRoTcan go for Neptune size planets or bigger in all its range of observation (down to R magnitude 16) and for planets as small as 2 Earth radii around stars brighter than R 14, although better performances can be achieved around brighter stars (as shown by CoRoT-7b).

However, we can check the performance of the survey in another empirical way, as done by Barge (2009) and Carpano et al. (2009). We can plot, as in Fig. 13, the depth of the candidates found by all teams in the LRc01 against the period of the candidate. In Fig. 13 we have superimposed the candidates in the LRc01 field the depths and periods of the 6+1 planetary-like objects discovered by CoRoT. A Neptune-like planet moving in front of a solar type star produces a transit of 0.1%, a regime that is well within the reach of CoRoT (for candidates with periods up to 10 days) as pointed out in the previous paragraph. However, planets like CoRoT-7b, which is shown in the bottom-left corner of the figure and which has a transit depth of 0.03%, can only be discovered around stars brighter than $R = 12$ (following the limits found in Aigrain et al. 2009). There are 317 of such targets in the LRa01(where CoRoT-7b was found), but only 95 in LRc01 (and among those, only 45 are dwarf stars). The targets in this run are fainter and present a larger fraction of giant stars than LRa01 targets (58% versus 22%, from Aigrain et al. 2009), which has to be considered when comparing the performances of both runs.

Several papers have been published measuring the performance of the detection algorithms as a function of the length of the run. These analyses were done on simulated data (see, for example, Defaÿ et al. 2001; Carpano & Fridlund 2008), and the main conclusion is that given a certain number of transits observed, the efficiency of the detection, measured as the smallest radius planet that can be detected around a given star, remains constant when more transits are observed.

In our context, the number of transits observed is given by the length of the run and the period of the target. We can study the efficiency of the detection algorithms as the fraction of candidates found in a shortened run compared to the total number of candidates known in the whole run. Here, a shortened run is built by reducing the length of the light curves; for example taking just the first 20, 40, 80, etc. days of observation. The results are given in Fig. 14. For example, analyzing only the first 80 days of the LRc01 we are able to find 94% of the candidates known in the whole run. Candidates in this context are again both binaries and planets. The detection algorithm finds a list of candidates and a posterior analysis, taking into account not only the significance of the signal, but also the information on the target star and the parameters of the candidate (period, duration, depth, color), in order to distinguish between potential planets and clear binaries.

With a *half run* of 80 days, we are able to detect a significant fraction of the candidates found in the whole set of data. But it has to be understood that by shortening a run we lose information: we lose precision in the determination of the ephemeris, so the follow-up is more difficult; we lose really long period candidates; we lose precision in the transit timing variation analysis, because those need the longest time base line available; the oversampled (32 s) fraction of the light curve for planet candidates is shorter, so the characterization of their physical parameters is not as precise as with a longer baseline, etc.

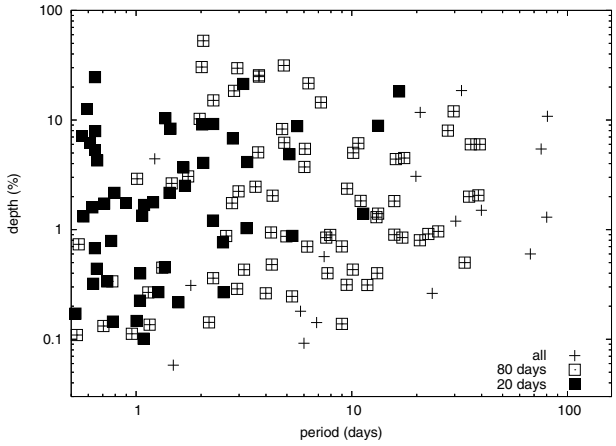

Fig. 15. Depths and periods of the candidates found in shortened runs of 20 and 80 days compared to the candidates found in the whole run.

Figure 15 shows a comparison of the depths and periods of the candidates found in different shortened runs. There are slight differences with Fig. 13 due to crowding effects and because the results presented in the comparative study are based only on the automatic pipeline of just one of the algorithms used by the detection teams. This diagram must not be used to make assertions on the detectability of a particular candidate, but as a tool for understanding the evolution of the efficiency of detection as a function of the length of the run (or, for a given period, the number of transits observed).

8. Summary

Table 3 summarizes the results of the follow-up effort done in the LRc01: 34 candidates with R magnitudes between 12 and 16 were followed up with different photometric and spectroscopic facilities. The nature of 26 candidates has been unambiguously established: 2 planets, 7 contaminating eclipsing binaries, 3 blends, 6 SB1, and 2 SB2. Six binaries were rejected by CoRoT photometry. Finally, 16 candidates are waiting for follow-up. As already pointed out by Moutou et al. (2009), the follow-up requires a huge effort and it is not always straightforward or conclusive at the faint end of the magnitude range.

Figures 12 and 13 allow the question to be addressed of the detection capabilities of CoRoT. The signal of planets as small as Neptune should be detected in all the observed magnitude range. However, so far CoRoT has only found relatively large planets (with the exception of CoRoT-7b) at the bright end of the observed sample. A priori, nothing in the analyzed data indicates a severe degradation of the photometric performances beyond the expected photon noise limitations. The lack of Neptune and Jupiter-like planets at the faint end might be for two main reasons: first, the spectroscopic follow-up of the candidates is more complicated, requires longer observations and is in the reach of fewer instruments (namely HARPS). Second, some binaries can be easily identified as such from CoRoT photometry due to the presence of a secondary. However, it is more difficult to find this secondary around faint targets because the signal-to-noise ratio is poorer, which possibly makes the contamination of binaries higher at the faint end, reducing the performance of the planet detection. Recently, Almenara et al. (2009) have published a detailed study evaluating the rates and nature of false positives in the first CoRoT fields observed, which also provides insight into the nature of the planetary populations detected with CoRoT. However, it cannot be discarded yet, as pointed out by Moutou et al. (2009), that there is an error found not in the detection of candidates, but in their selection: hence, good planetary candidates would have been rejected as binaries just from the analysis of photometric data because of a bad estimation of the planet parameters caused by poor knowledge of a faint host star. The possibility of a real lack of Jupiters around faint stars does not seem to have any physical basis.

For the 2 Earth radii limit, the constraints imposed by the photon noise limit are severe, and in the case of the LRc01, there is a lack of dwarf stars in the observed sample, which reduces the population of suitable targets for the planet search, hence the number of possible positive detections.

Acknowledgements. H.J.D., J.M.A., and M.R. acknowledge support by grants ESP2004-03855-C03-03 and ESP2007-65480-C02-02 of the Spanish Ministerio de Ciencia e Innovación. D.G. acknowledges the support of grant 50OW0204 from the Deutschen Zentrums für Luft- und Raumfahrt (DLR). T.M. acknowledges support from the Israel Science Foundation (grant No. 655/07).
Some of the data published in this article were acquired with the IAC80 telescope operated by the Instituto de Astrofísica de Canarias in the Observatorio del Teide, and special thanks is given to its staff for performing a large fraction of these observations. Part of the observations presented in this paper were performed with the 2.1 m Otto Struve telescope operated at McDonald Observatory, and with the 2 m Alfred Jensch telescope at the Thüringer Landessternwarte Tautenburg. This research has made use of the Exo-Dat database, operated at LAM-OAMP, Marseille, France, on behalf of the CoRoT/Exoplanet program, whose input catalog was made possible thanks to observations collected for years at the Isaac Newton Telescope (INT), operated on the island of La Palma by the Isaac Newton group in the Spanish Observatorio del Roque de Los Muchachos of the Instituto de Astrofísica de Canarias.
This publication made use of NASA's Astrophysics Data System Bibliographic Services and of data products from the Two Micron All Sky Survey, which is a joint project of the University of Massachusetts and the Infrared Processing and Analysis Center/California Institute of Technology, funded by the National Aeronautics and Space Administration and the National Science Foundation.

References

Aigrain, S., Collier Cameron, A., Ollivier, M., et al. 2008, A&A, 488, L43
Aigrain, S., Pont, F., Fressin, F., et al. 2009, A&A, 506, 425
Alapini, A., & Aigrain, S. 2008, in IAU Symp. 249, ed. Y.-S. Sun, S. Ferraz-Mello, & J.-L. Zhou, 89
Almenara, J. M., Deeg, H. J., Aigrain, S., et al. 2009, A&A, 506, 337
Alonso, R., Auvergne, M., Baglin, A., et al. 2008, A&A, 482, L21
Auvergne, M., Bodin, P., Boisnard, L., et al. 2009, A&A, 506, 411
Baglin, A., Auvergne, M., Boisnard, L., et al. 2006, in COSPAR, Plenary Meeting, 36, 36th COSPAR Scientific Assembly, 3749
Barge, P. 2009, in IAU Symp., 253, 83
Barge, P., Baglin, A., Auvergne, M., et al. 2008a, A&A, 482, L17
Barge, P., Baglin, A., Auvergne, M., & the CoRoT team. 2008b, in IAU Symp., 249, 3
Baudin, F., Baglin, A., Orcesi, J.-L., et al. 2006, in ESA SP-1306, ed. M. Fridlund, A. Baglin, J. Lochard, & L. Conroy, 145
Boisnard, L., & Auvergne, M. 2006, in ESA SP-1306, ed. M. Fridlund, A. Baglin, J. Lochard, & L. Conroy, 19
Bordé, P., Fressin, F., Ollivier, M., Léger, A., & Rouan, D. 2007, in Transiting Extrapolar Planets Workshop, ed. C. Afonso, D. Weldrake, & T. Henning, ASP Conf. Ser., 366, 145
Bouchy, F., Queloz, D., Deleuil, M., et al. 2008, A&A, 482, L25
Burgasser, A. J., Dhital, S., & West, A. 2009, AJ, accepted [arXiv:0909.3885]
Burrows, A., Hubbard, W. B., Lunine, J. I., & Liebert, J. 2001, Rev. Mod. Phys., 73, 719
Carpano, S., & Fridlund, M. 2008, A&A, 485, 607
Carpano, S., Cabrera, J., Alonso, R., et al. 2009, A&A, 506, 491
Claret, A. 1998, A&A, 335, 647
Claret, A. 2000, A&A, 363, 1081
de Ridder, J., Barban, C., Baudin, F., et al. 2009, Nature, 459, 398
Debosscher, J., Sarro, L. M., López, M., et al. 2009, A&A, 506, 519
Deeg, H. J., Gillon, M., Shporer, A., et al. 2009, A&A, 506, 343
Defaÿ, C., Deleuil, M., & Barge, P. 2001, A&A, 365, 330

Deleuil, M., Deeg, H. J., Alonso, R., et al. 2008, A&A, 491, 889
Deleuil, M., Meunier, J. C., Moutou, C., et al. 2009, AJ, 138, 649
Drummond, R., Lapeyrere, V., Auvergne, M., et al. 2008, A&A, 487, 1209
Gandolfi, D., Alcalá, J. M., Leccia, S., et al. 2008, ApJ, 687, 1303
Gondoin, P., et al. 2009, in Conf. proc. Cool Stars, 15
Hekker, S., Kallinger, T., Baudin, F., et al. 2009, A&A, 506, 465
Karoff, C., Rauer, H., Erikson, A., et al. 2007, AJ, 134, 766
Lanza, A. F., Pagano, I., Leto, G., et al. 2009, A&A, 493, 193
Léger, A., Rouan, D., Schneider, J., et al. 2009, A&A, 506, 287
Llebaria, A., & Guterman, P. 2006, in ESA SP-1306, ed. M. Fridlund, A. Baglin, J. Lochard, & L. Conroy, 293
Mandel, K., & Agol, E. 2002, ApJ, 580, L171
Mazeh, T., Guterman, P., Aigrain, S., et al. 2009, A&A, 506, 431
Meunier, J.-C., Deleuil, M., Moutou, C., et al. 2007, in Astronomical Data Analysis Software and Systems XVI, ed. R. A. Shaw, F. Hill, & D. J. Bell, ASP Conf. Ser., 376, 339
Michel, E., Baglin, A., Weiss, W. W., et al. 2008, Commun. Asteroseismol., 157, 69
Moutou, C., Pont, F., Barge, P., et al. 2005, A&A, 437, 355
Moutou, C., Aigrain, S., Almenara, J., et al. 2007, in Transiting Extrapolar Planets Workshop, ed. C. Afonso, D. Weldrake, & T. Henning, ASP Conf. Ser., 366, 127
Moutou, C., Bruntt, H., Guillot, T., et al. 2008, A&A, 488, L47
Moutou, C., Pont, F., Bouchy, F., et al. 2009, A&A, 506, 321
Pinheiro da Silva, L., Rolland, G., Lapeyrere, V., & Auvergne, M. 2008, MNRAS, 384, 1337
Pont, F., Bouchy, F., Melo, C., et al. 2005, A&A, 438, 1123
Pont, F., Zucker, S., & Queloz, D. 2006, MNRAS, 373, 231
Press, W. H., Teukolsky, S. A., Vetterling, W. T., & Flannery, B. P. 2002, Numerical Recipes in C++, 2nd edn. (Cambridge University Press)
Rauer, H., Queloz, D., Csizmadia, Sz., et al. 2009, A&A, 506, 281
Régulo, C., Almenara, J. M., Alonso, R., Deeg, H., & Roca Cortés, T. 2007, A&A, 467, 1345
Renner, S., Rauer, H., Erikson, A., et al. 2008, A&A, 492, 617
Seager, S., & Mallén-Ornelas, G. 2003, ApJ, 585, 1038
Surace, C., Alonso, R., Barge, P., et al. 2008, in SPIE Conf., 7019
Torres, G., Winn, J. N., & Holman, M. J. 2008, ApJ, 677, 1324
Wilson, R. E., & Devinney, E. J. 1971, ApJ, 166, 605

Table 3. Follow-up instruments used to solve the nature of the candidates in the LRc01.

CoRoTid	Winid	*R*	Nature of the candidate	Follow-up facilities
101368192	E1_0523	13.099	CoRoT-3b	OGS, SOPHIE, Wise, BEST, IAC80, HARPS, TLS, McDonald
101206560	E2_0192	12.204	CoRoT-2b	IAC, Wise, SOPHIE, HARPS
100567226	E2_5365	15.519	SB1	HARPS, FLAMES
110604224	E2_3681	15.261	CEB	EULER, IAC80
101351899	E2_0305	12.813	SB1	SOPHIE
101436549	E1_3129	14.887	CEB	IAC80, TLS
101068850	E1_0769	13.511	SB2	SOPHIE
100589010	E2_4006	15.379	CEB	HARPS, Wise
100609705	E2_3895	15.313	CEB	EULER, IAC80
101653417	E1_1253	13.988	blend	HARPS, SOPHIE
100982006	E1_1090	13.643	SB1	SOPHIE
101708400	E1_2936	14.788	SB1	FLAMES
101482707	E1_2837	12.969	SB2	SOPHIE
101031117	E2_0840	13.644	SB1	SOPHIE
100773735	E2_1245	13.740	SB1(?)	SOPHIE
101259269	E1_5626	15.421	binary	*rejected from CoRoT photometry*
101218359	E1_1845	14.612	binary	*rejected from CoRoT photometry*
100468104	E2_2533	14.733	binary	*rejected from CoRoT photometry*
100834293	E2_5414	15.948	binary	IAC80, *rejected from CoRoT photometry*
101026464	E1_5745	15.937	binary	*rejected from CoRoT photometry*
101434308	E1_3425	14.477	binary	*rejected from CoRoT photometry*
101106246	E2_3257	15.345	CEB	EULER, IAC80
101095286	E1_2376	11.907	CEB	Wise, IAC80
101175376	E1_4959	15.377	CEB	IAC80
101055792	E1_2140	14.570	blend	IAC80, SOPHIE, HARPS, TLS
101675703	E1_4863	14.765	blend	HARPS
101086161	E2_1145	14.267	unknown	SOPHIE, OHP, HARPS
100905839	E2_5801	15.673	unknown	HARPS, UVES
100725706	E2_1802	13.744	unknown	HARPS
101206989	E1_1929	14.449	unknown	IAC80, SOPHIE, HARPS, TLS
101332685	E2_3345	15.250	unknown	HARPS
101186644	E1_4780	15.670	unknown	HARPS
101157411	E1_0715	13.308	unknown	SOPHIE, UVES
101123916	E2_4295	15.868	unknown	OGS, CFHT
101424939	E1_1632	14.490	unknown	EULER
100768215	E2_4390	15.875	unknown	IAC80, CFHT
100887662	E2_0934	13.812	unknown	*not started*
100980128	E1_0673	13.155	unknown	TLS
101439653	E1_2761	14.758	unknown	*not started*
101115531	E1_1791	14.436	unknown	*not started*
100654833	E2_4241	14.577	unknown	FLAMES
101614469	E1_2278	13.880	unknown	HARPS, TLS

Table 4. Parameters of the candidates in ongoing follow-up.

pr	CoRoTid	Winid	Right ascension (J2000.0)	Declination (J2000.0)	*B*	*V*	*R*	*I*	Period(d)	Epoch (HJD-2 454 000)	Depth (%)	Length (h)
1	101086161	E2_1145	19 26 21.25	4 25 35.3	16.096	14.797	14.267	13.408	6.212242 ± 0.000013	282.5214 ± 0.0007	0.69	2.3
2	100905839	E2_5801	19 25 13.09	1 23 35.0	17.483	16.188	15.673	14.903	15.74179 ± 0.00004	252.8484 ± 0.0025	0.74	3.9
2	100725706	E2_1802	19 24 15.27	0 44 46.0	16.676	15.216	14.730	13.744	13.24043 ± 0.00022	273.3452 ± 0.0012	1.18	2.2
4	101206989	E1_1929	19 27 06.65	0 03 24.7	16.308	15.012	14.449	13.706	0.577855 ± 0.000025	237.3629 ± 0.0042	0.30	1.3
3	101332685	E2_3345	19 27 55.77	1 38 06.6	17.145	15.767	15.25	14.326	13.0995 ± 0.0050	264.9936 ± 0.0050	0.48	3.6
2	101186644	E1_4780	19 30 59.09	0 29 06.4	17.092	16.049	15.670	14.934	40.3680 ± 0.0035	240.3230 ± 0.0067	0.86	5.9
3	101157411	E1_0715	19 26 48.06	−0 06 49.8	14.426	13.648	13.308	12.822	single transit	293.9028 ± 0.0050	0.60	9.0
3	101123916	E2_4295	19 26 35.46	2 05 53.6	17.872	16.449	15.868	15.048	1.13828 ± 0.00050	245.6150 ± 0.0050	0.28	2.9
3	101424939	E1_1632	19 28 37.92	0 46 42.5	15.864	14.856	14.490	13.735	2.177256 ± 0.000033	237.7746 ± 0.0014	0.14	1.2
3	100768215	E2_4390	19 24 29.57	0 49 56.3	18.062	16.464	15.875	14.862	2.93896 ± 0.00019	237.8604 ± 0.0074	0.30	4.1
4	100887662	E2_0934	19 25 07.34	1 29 37.5	14.938	14.138	13.812	13.247	single transit	322.2757 ± 0.0050	2.28	8.6
4	100980128	E1_0673	19 25 36.90	0 22 34.5	14.471	13.516	13.155	12.539	6.00234 ± 0.00050	250.8702 ± 0.0050	0.09	2.9
3	101439653	E1_2761	19 28 44.04	−0 10 03.8	16.139	15.175	14.758	14.245	17.49731 ± 0.00050	246.1441 ± 0.0050	4.11	3.1
4	101115531	E1_1791	19 26 32.28	0 29 37.6	16.252	14.924	14.436	13.524	0.520959 ± 0.00050	237.0493 ± 0.0050	0.18	0.96
3	100654833	E2_4241	19 23 45.92	1 14 18.6	17.283	15.938	15.351	14.577	0.53108 ± 0.00050	236.8081 ± 0.0050	0.11	2.3
3	101614469	E1_2278	19 29 56.79	0 05 53.3	16.591	15.231	14.673	13.880	6.86934 ± 0.00067	242.0216 ± 0.0095	0.16	6.1

Table 5. Parameters of the candidates solved by the follow-up. The values for the period and epoch for CoRoT-2b and CoRoT-3b have been taken from the literature.

pr	CoRoTid	Winid	Right ascension (J2000.0)	Declination (J2000.0)	*B*	*V*	*R*	*I*	Period(d)	Epoch (HJD-2 454 000)	Depth (%)	Length (h)	Follow-up result
1	101368192	E1_0523	19 28 13.26	0 07 18.7	14.199	13.292	13.099	12.676	4.25680 ± 0.000005	283.1383 ± 0.0003	0.45	3.5	CoRoT-3b
1	101206560	E2_0192	19 27 06.50	1 23 01.5	13.422	12.568	12.204	11.641	1.7429964 ± 0.0000017	237.5356 ± 0.0007	2.9	1.9	CoRoT-2b
1	100567226	E2_5365	19 23 15.71	1 18 45.2	17.089	15.974	15.519	14.861	7.70975 ± 0.00001	244.3781 ± 0.0001	0.47	1.8	SB1
1	110604224	E2_3681	19 24 02.74	0 49 07.6	16.752	15.684	15.261	14.471	3.45075 ± 0.00001	240.5668 ± 0.0001	0.15	2.8	CEB
2	101351899	E2_0305	19 28 05.19	1 22 23.7	13.819	13.079	12.813	12.330	21.97190 ± 0.00069	239.0418 ± 0.0021	0.93	3.6	SB1
3	101436549	E1_3129	19 28 42.75	0 33 45.0	15.984	15.204	14.887	14.750	0.73495 ± 0.00050	237.2723 ± 0.0050	0.30	1.4	CEB
4	101068850	E1_0769	19 26 13.35	0 39 35.2	15.194	14.007	13.511	12.632	single transit	294.4770 ± 0.0050	4.0	7.2	SB2
3	100589010	E2_4006	19 31 23.52	1 16 22.7	17.243	15.934	15.379	14.591	0.78053 ± 0.00050	241.0131 ± 0.0050	0.14	2.0	CEB
2	100609705	E2_3895	19 31 30.84	1 14 32.6	16.968	15.813	15.313	14.685	3.30382 ± 0.00001	242.8553 ± 0.0001	0.09	4.0	CEB
3	101653417	E1_1253	19 30 17.21	0 09 32.9	16.027	14.591	13.988	13.215	5.77991 ± 0.00050	239.0721 ± 0.0050	0.15	2.5	blend
3	100982006	E1_1090	19 25 37.52	0 10 31.0	15.039	14.052	13.643	13.092	16.68904 ± 0.00050	236.9460 ± 0.0050	0.40	3.8	SB1
3	101708400	E1_2936	19 30 40.09	−0 01 08.9	16.436	15.256	14.788	14.165	4.220221 ± 0.000015	279.2119 ± 0.0009	0.85	5.1	SB1
2	101482707	E1_2837	19 29 01.57	0 37 12.2	14.474	13.366	12.969	12.256	39.8883 ± 0.0001	260.2825 ± 0.00013	1.31	4.9	SB2
3	101031117	E2_0840	19 25 56.12	1 32 00.5	14.767	13.937	13.644	13.008	107.5878 ± 0.0067	313.4829 ± 0.0048	0.60	3.8	SB1
2	100773735	E2_1245	19 24 31.35	1 13 15.9	14.837	14.056	13.740	13.232	4.973876 ± 0.000008	279.5044 ± 0.0004	0.66	4.4	SB2
4	101259269	E1_5626	19 27 26.48	0 45 03.5	17.414	15.942	15.421	14.437	4.43324 ± 0.00025	240.9053 ± 0.0055	0.21	4.8	binary
4	101218359	E1_1845	19 27 10.96	−0 27 50.3	16.599	15.196	14.612	13.855	1.154871 ± 0.000024	237.6010 ± 0.0015	0.13	1.0	binary
4	100468104	E2_2533	19 22 40.22	1 34 06.8	16.390	15.228	14.733	14.032	1.043594 ± 0.000009	237.0941 ± 0.0007	0.32	1.6	binary
4	100834293	E2_5414	19 24 50.46	1 45 11.4	17.308	16.358	15.948	15.268	11.301870 ± 0.000024	275.8783 ± 0.0013	0.90	2.3	binary
4	101026464	E1_5745	19 25 54.05	−0 17 24.5	17.174	16.311	15.937	15.425	1.322011 ± 0.000019	238.1208 ± 0.0012	0.40	1.1	binary
4	101434308	E1_3425	19 28 41.80	−0 24 09.5	15.659	14.846	14.477	14.035	79.9808 ± 0.0005	280.6340 ± 0.0050	2.7	10.0	binary
2	101106246	E2_3257	19 26 28.79	1 00 45.6	17.639	15.983	15.345	14.389	11.31662 ± 0.00007	252.7348 ± 0.0043	0.33	3.6	CEB
4	101095286	E1_2376	19 26 24.66	0 36 06.1	15.294	13.552	12.986	11.907	10.10655 ± 0.00050	241.2432 ± 0.0050	0.25	4.2	CEB
4	101175376	E1_4959	19 26 54.86	−0 10 56.9	16.554	15.731	15.377	14.850	5.28013 ± 0.00031	239.0282 ± 0.0005	0.41	11.9	CEB
1	101055792	E1_2140	19 26 07.32	0 16 31.6	16.400	15.112	14.570	13.836	1.9384 ± 0.0001	237.6745 ± 0.0001	0.13	2.0	blend
1	101675703	E1_4863	19 30 26.34	0 01 09.9	17.424	16.091	15.487	14.765	1.79308 ± 0.00050	238.0019 ± 0.0050	0.29	2.4	blend

Table 6. Eclipsing binaries found in LRc01.

CoRoTid	Winid	Right ascension (J2000.0)	Declination (J2000.0)	*B*	*V*	*R*	*I*	Period(d)	Epoch (HJD-2 454 000)	Length (h)	Depth (%)
100493215	E2_3956	19 22 49.06	1 23 15.7	16.686	15.531	15.043	14.345	10.14815 ± 0.000179	240.603937 ± 0.001461	9.1	3.5
100524672	E2_4093	19 23 00.29	1 20 39.0	17.203	16.081	15.593	14.918	0.432501 ± 0.000006	236.664268 ± 0.000963	2.74	11.0
100534603	E2_1954	19 23 03.82	1 47 48.1	16.512	14.955	14.326	13.492	34.97716 ± 0.000232	270.425379 ± 0.003467	8.3	1.4
100542479	E2_4680	19 23 06.71	1 20 09.6	16.916	15.911	15.480	14.858	single eclipse	263.886 ± 0.005	8.4	4.0
100552362	E2_4218	19 23 10.26	1 22 37.6	16.453	15.588	15.236	14.705	1.347553 ± 0.000010	237.988331 ± 0.000556	12.0	1.9
100567689	E2_5511	19 23 15.87	1 32 25.7	17.150	16.051	15.573	14.938	10.723641 ± 0.000099	246.366724 ± 0.000651	7.0	4.4
100583369	E2_3526	19 23 21.50	1 42 25.4	17.541	16.004	15.350	14.502	0.323345 ± 0.000005	237.391753 ± 0.000616	1.35	3.2
100587133	E2_4820	19 23 22.84	1 09 47.3	17.534	16.314	15.814	15.101	2.614110 ± 0.000045	239.260664 ± 0.001400	6.4	0.9
100588558	E2_2864	19 23 23.37	1 22 39.4	16.666	15.528	15.013	14.268	0.574973 ± 0.000008	237.594196 ± 0.001130	2.6	0.4
100588681	E2_4283	19 23 23.42	1 38 06.5	14.872	13.914	12.961	12.382	0.793329 ± 0.000002	237.749591 ± 0.000160	2.3	2.7
100621853	E2_5219	19 23 34.89	1 21 24.3	17.107	16.064	15.615	14.970	0.927198 ± 0.000012	237.746399 ± 0.000946	1.71	0.2
100622251	E2_2631	19 23 35.02	1 40 58.7	16.954	15.531	14.908	14.052	32.356577 ± 0.002166	262.310852 ± 0.004337	7.65	0.7
100624108	E2_5789	19 23 35.64	1 02 55.0	18.195	16.573	15.871	14.993	0.645860 ± 0.000006	237.532236 ± 0.000793	3.37	8.8
100640794	E2_3828	19 23 41.18	1 20 38.6	16.361	15.422	15.001	14.382	0.259409 ± 0.000001	237.257605 ± 0.000163	3.00	2.7
100649547	E2_5020	19 23 44.10	1 15 43.8	18.338	16.683	15.977	15.089	0.441601 ± 0.000002	237.298447 ± 0.000321	3.54	5.6
100657980	E2_1661	19 23 47.09	1 35 12.0	16.508	15.308	14.698	13.913	21.930339 ± 0.000180	258.132498 ± 0.000511	8.4	20.7
100674412	E2_4423	19 23 53.75	1 32 03.2	17.508	16.388	15.853	15.068	1.197550 ± 0.000004	238.009520 ± 0.000229	2.4	1.7
110567660	E2_1868	19 23 56.49	0 46 35.7	15.958	15.028	14.676	13.991	1.239046 ± 0.000012	238.080326 ± 0.000766	11.0	0.5
100682721	E2_5407	19 23 57.12	1 45 22.2	17.078	16.101	15.723	15.015	1.855369 ± 0.000007	238.911613 ± 0.000298	7.3	20.8
100695831	E2_5524	19 24 02.47	1 19 18.9	17.537	16.451	15.982	15.353	1.088648 ± 0.000005	238.132476 ± 0.000397	3.03	1.6
100705717	E2_0667	19 24 06.52	1 19 40.1	15.367	14.031	13.472	12.733	13.01342 ± 0.000019	242.919066 ± 0.000121	2.9	1.0
100707214	E2_3570	19 24 07.14	1 40 14.1	15.708	15.113	14.843	14.283	2.783760 ± 0.000027	239.556950 ± 0.000754	3.06	1.9
100717622	E2_5567	19 24 11.43	1 04 28.0	16.837	15.811	15.372	14.733	2.280295 ± 0.000010	239.258369 ± 0.000338	9.3	12.8
100726311	E2_2130	19 24 15.64	1 41 23.0	16.629	15.295	14.693	13.722	0.412113 ± 0.000006	236.990182 ± 0.000100	3.8	0.95
100749711	E2_0520	19 24 23.56	1 39 38.1	14.663	13.768	13.418	12.719	1.461617 ± 0.000004	238.626863 ± 0.000232	5.7	2.6
100753487	E2_1078	19 24 24.77	1 58 58.3	15.057	14.287	14.007	13.504	1.011423 ± 0.000004	237.788987 ± 0.000346	3.3	8.8
100758671	E2_0379	19 24 26.48	0 58 18.2	12.967	12.521	12.389	12.120	single eclipse	238.128 ± 0.005	9.0	12.7
100767569	E2_3910	19 24 29.35	0 52 46.5	16.071	14.239	13.555	12.492	2.983335 ± 0.000020	240.225460 ± 0.000489	9.7	1.8
100768113	E2_5563	19 24 29.53	1 06 03.3	16.632	15.016	14.335	13.387	0.328903 ± 0.000001	237.321154 ± 0.000177	3.8	6.0
100773527	E1_2325	19 24 31.28	0 28 26.5	16.009	15.069	14.681	13.991	1.793424 ± 0.000034	238.792951 ± 0.001658	3.28	0.1
100787846	E2_0507	19 24 35.83	1 14 56.5	15.147	13.901	13.385	12.672	39.199640 ± 0.000410	263.386223 ± 0.000751	7.2	6.2
100794107	E2_3582	19 24 37.81	1 08 08.9	17.212	15.896	15.356	14.566	0.604346 ± 0.000007	237.610021 ± 0.000808	1.32	0.1
100805120	E2_0271	19 24 41.27	0 37 13.6	15.066	13.546	13.120	12.154	2.271684 ± 0.000008	239.419524 ± 0.000271	4.1	1.6
100811279	E2_2752	19 24 43.20	1 12 37.6	16.667	15.521	15.029	14.340	0.339217 ± 0.000007	237.652542 ± 0.001572	2.5	1.2
100813794	E2_0401	19 24 44.02	1 42 21.3	14.299	13.438	13.133	12.498	1.083353 ± 0.000011	237.610906 ± 0.000859	1.40	0.1

Table 6. continued.

CoRoTid	Winid	Right ascension (J2000.0)	Declination (J2000.0)	*B*	*V*	*R*	*I*	Period(d)	Epoch (HJD-2 454 000)	Length (h)	Depth (%)
100818164	E1_1319	19 24 45.40	0 27 31.8	15.419	14.409	14.066	13.340	0.306873 ± 0.000001	237.275349 ± 0.000172	2.7	3.8
100841854	E2_2257	19 24 52.84	0 39 44.2	16.706	15.096	14.620	13.614	17.148499 ± 0.000577	248.843315 ± 0.002438	2.31	0.4
100851348	E1_2214	19 24 55.87	0 19 45.0	15.867	14.913	14.591	13.976	0.854829 ± 0.000004	237.713793 ± 0.000440	8.7	1.6
100866999	E2_1719	19 25 00.78	0 54 41.1	15.867	14.971	14.599	13.980	2.808769 ± 0.000022	239.396628 ± 0.000656	3.9	6.7
100871572	E2_0170	19 25 02.22	1 41 43.9	13.964	12.683	12.208	11.389	0.301518 ± 0.000001	237.293159 ± 0.000178	2.7	0.6
100871803	E1_3671	19 25 02.31	0 18 52.9	16.563	15.502	15.086	14.447	7.439679 ± 0.000202	243.026515 ± 0.002314	2.59	0.4
100878452	E2_4445	19 25 04.40	1 05 41.0	17.972	16.486	15.871	14.972	1.359027 ± 0.000018	238.398893 ± 0.001068	2.29	0.4
100880613	E2_0431	19 25 05.10	1 38 50.7	15.123	14.588	14.413	13.964	0.893160 ± 0.000006	237.638648 ± 0.000542	9.4	1.9
100883990	E2_4314	19 25 06.18	1 50 51.1	16.968	15.871	15.433	15.205	0.848685 ± 0.000008	237.619000 ± 0.000751	1.10	0.2
100885002	E2_4653	19 25 06.49	1 50 31.3	15.938	14.610	14.086	13.327	11.808625 ± 0.000626	248.643047 ± 0.004115	5.04	0.5
100898207	E2_3579	19 25 10.68	1 52 33.8	16.164	15.453	15.196	14.640	6.030804 ± 0.000109	242.749856 ± 0.001339	5.85	3.1
100906796	E2_0663	19 25 13.40	1 57 10.6	14.172	13.597	13.427	13.075	0.897635 ± 0.000006	237.431242 ± 0.000504	8.6	1.5
100920405	E2_0377	19 25 17.80	1 42 58.2	15.069	14.635	14.463	13.972	1.009714 ± 0.000006	238.038765 ± 0.000444	10.0	3.3
100921311	E1_0777	19 25 18.09	0 29 12.6	15.609	13.954	13.330	12.371	2.527714 ± 0.000017	239.053641 ± 0.000557	3.9	0.76
100934790	E1_4048	19 25 22.39	0 17 38.3	17.588	16.437	15.966	15.282	0.276416 ± 0.000005	237.099950 ± 0.000901	0.60	0.6
100945095	E2_3518	19 25 25.73	1 19 11.8	17.152	15.616	14.970	14.107	0.614208 ± 0.000002	237.499276 ± 0.000266	2.47	5.5
100950734	E2_5104	19 25 27.54	0 44 23.0	17.156	15.906	15.550	14.644	0.409350 ± 0.000002	237.368086 ± 0.000362	3.54	0.9
100953598	E2_4803	19 25 28.46	1 42 00.8	17.245	16.058	15.603	14.798	1.428578 ± 0.000004	238.078203 ± 0.000218	1.81	1.9
100960211	E2_0545	19 25 30.60	0 42 43.1	14.785	13.771	13.476	12.748	0.351817 ± 0.000001	237.225451 ± 0.000260	2.0	4.4
100964052	E2_4946	19 25 31.81	0 57 40.6	17.851	16.406	15.749	14.938	0.718631 ± 0.000006	237.411966 ± 0.000662	2.21	0.3
100964422	E2_2907	19 25 31.93	1 37 20.9	16.305	15.394	15.013	14.337	3.272218 ± 0.000011	240.274119 ± 0.000271	3.0	3.7
100966880	E2_0747	19 25 32.69	2 07 02.5	15.497	15.019	14.852	14.614	2.843947 ± 0.000011	239.380054 ± 0.000301	7.5	16.0
100972787	E2_3478	19 25 34.57	1 31 47.2	16.443	15.541	15.163	14.569	0.657350 ± 0.000005	237.831740 ± 0.000575	3.54	0.4
100998053	E1_2588	19 25 42.68	−0 10 37.1	16.121	15.314	14.944	14.468	0.374290 ± 0.000004	237.765186 ± 0.000448	4.0	27.4
100999813	E1_5271	19 25 43.25	−0 05 06.0	17.270	16.228	15.763	15.126	4.839209 ± 0.000015	240.264993 ± 0.000267	8.2	25.3
101006984	E2_1872	19 25 45.65	1 00 38.1	15.985	15.050	14.619	14.026	0.621098 ± 0.000007	237.672371 ± 0.000774	5.56	0.2
101010567	E2_3938	19 25 47.02	1 40 35.3	16.626	15.850	15.559	14.899	0.495335 ± 0.000003	237.404572 ± 0.000471	5.2	5.1
101012476	E1_4075	19 25 47.84	−0 02 05.8	16.351	15.522	15.160	14.627	1.267792 ± 0.000013	237.769380 ± 0.000884	1.43	0.3
101013351	E1_2433	19 25 48.24	−0 17 18.6	16.314	15.201	14.717	14.065	1.066879 ± 0.000002	237.886537 ± 0.000186	1.8	1.8
101014035	E2_0249	19 25 48.54	1 53 21.6	15.227	14.504	14.208	13.718	0.459684 ± 0.000002	237.483596 ± 0.000370	4.4	6.6
101017242	E1_2297	19 25 49.94	0 11 20.0	15.986	14.932	14.465	13.826	17.807563 ± 0.000111	251.946708 ± 0.000558	4.2	5.9
101018658	E1_2978	19 25 50.57	−0 12 08.4	16.014	15.171	14.817	14.315	7.190920 ± 0.000036	243.888828 ± 0.000355	6.2	12.9
101020215	E2_1450	19 25 51.28	1 29 13.5	16.127	15.057	14.654	13.928	0.431121 ± 0.000001	237.476193 ± 0.000259	1.68	14.1
101021491	E2_2192	19 25 51.84	1 21 29.9	17.340	15.761	15.117	14.128	0.562694 ± 0.000004	236.889077 ± 0.000571	6.0	8.0
101027599	E2_3995	19 25 54.56	0 49 38.1	15.924	14.167	13.551	12.492	24.326642 ± 0.003431	257.253674 ± 0.008592	9.0	0.4
101030167	E2_2861	19 25 55.69	1 44 38.0	16.886	15.433	14.834	13.831	5.139099 ± 0.000017	241.655497 ± 0.000259	4.0	3.9
101041026	E2_2871	19 26 00.60	2 07 05.6	16.828	15.435	14.852	14.154	7.941073 ± 0.000168	242.032442 ± 0.001707	2.72	0.9
101044194	E2_0436	19 26 02.04	1 38 11.0	15.406	14.020	13.464	12.494	8.811449 ± 0.000288	245.541524 ± 0.002181	22.5	21.0
101046418	E2_3462	19 26 03.05	1 47 18.0	17.546	16.213	15.624	14.651	3.164328 ± 0.000061	238.808199 ± 0.001466	2.65	0.4
101046635	E2_5781	19 26 03.15	1 59 05.6	17.268	16.325	15.882	15.364	7.866583 ± 0.000159	242.541463 ± 0.001592	2.62	0.9
101059693	E1_3210	19 26 09.09	0 36 13.3	17.279	15.857	15.376	14.472	0.644117 ± 0.000002	237.301447 ± 0.000258	1.24	0.7
101060029	E2_5794	19 26 09.24	1 15 41.1	16.164	14.656	14.039	13.109	25.169421 ± 0.002154	259.511008 ± 0.006209	5.63	1.0
101065348	E1_0499	19 26 11.70	−0 02 46.1	13.961	13.282	12.980	12.527	4.862924 ± 0.000029	241.747096 ± 0.000491	3.2	6.2
101068234	E2_5665	19 26 13.04	1 46 18.3	16.836	15.043	14.284	13.001	26.630938 ± 0.004802	257.882296 ± 0.012796	6.12	0.5
101075429	E2_4987	19 26 17.21	2 01 30.8	16.448	14.895	14.232	13.434	3.249819 ± 0.000024	240.272284 ± 0.000558	2.9	3.6
101078082	E2_5777	19 26 18.19	1 02 20.8	15.738	14.774	14.426	13.732	0.631924 ± 0.000004	237.393039 ± 0.000499	1.16	0.2
101078725	E1_2851	19 26 18.42	0 03 46.1	16.202	15.272	14.872	14.316	0.641844 ± 0.000003	237.093398 ± 0.000440	2.6	6.3
101084062	E2_3293	19 26 20.47	1 17 35.4	16.139	14.403	13.634	12.578	0.855876 ± 0.000023	237.920122 ± 0.002050	5.7	0.7
101091849	E1_5173	19 26 23.39	0 09 08.0	17.756	16.272	15.675	14.877	23.59258 ± 0.000114	254.469868 ± 0.003037	14	1.5
101092471	E2_4013	19 26 23.64	1 17 35.2	17.154	16.008	15.504	14.753	0.297700 ± 0.000001	237.367721 ± 0.000206	1.9	3.7
101098968	E2_1613	19 26 26.04	1 04 23.1	16.454	15.024	14.453	13.529	13.23131 ± 0.000013	250.258937 ± 0.000069	18.2	22.8
101103460	E1_0398	19 26 27.77	−0 26 01.0	14.989	14.451	14.247	13.895	2.014213 ± 0.000005	238.517286 ± 0.000207	5.2	26.7
101109378	E2_5245	19 26 29.96	1 35 33.8	17.339	16.362	15.976	15.226	5.580372 ± 0.000027	241.566001 ± 0.000359	4.3	7.7
101122252	E2_2209	19 26 34.83	2 06 24.2	16.228	15.215	14.782	14.234	2.276862 ± 0.000010	238.774050 ± 0.000367	4.8	9.1
101125371	E2_0713	19 26 35.99	1 40 31.8	15.001	13.985	13.614	12.830	1.003912 ± 0.000012	237.902275 ± 0.000915	1.74	0.2
101126445	E2_0643	19 26 36.41	2 13 31.2	15.438	14.175	13.612	12.914	29.66708 ± 0.000940	249.550000 ± 0.020422	49	12
101129018	E2_3052	19 26 37.40	1 52 56.5	16.390	15.018	14.433	13.531	0.285957 ± 0.000001	237.258762 ± 0.000146	2.1	20.6
101130839	E1_4583	19 26 38.06	0 24 55.5	16.937	15.914	15.545	14.854	13.049882 ± 0.000754	243.823412 ± 0.003602	2.19	0.6
101150514	E1_0226	19 26 45.46	0 15 24.3	12.790	12.297	12.130	11.796	0.523151 ± 0.000003	237.377985 ± 0.000416	3.13	0.1
101157705	E2_2750	19 26 48.16	0 58 36.5	16.805	15.418	14.865	14.004	19.81742 ± 0.038019	250.680000 ± 0.09375	25.0	5.0
101166793	E2_5556	19 26 51.64	1 02 47.0	15.554	14.621	14.250	13.596	6.296752 ± 0.000020	241.364792 ± 0.000252	7.2	17.8
101167963	E2_4273	19 26 52.07	1 46 17.4	17.542	16.225	15.729	14.799	4.494954 ± 0.000014	241.079695 ± 0.000203	4.07	0.6
101169499	E1_4392	19 26 52.64	−0 23 16.4	16.859	15.921	15.527	14.945	1.207098 ± 0.000018	238.103207 ± 0.001207	1.4	0.09
101172008	E2_4406	19 26 53.61	1 07 11.6	17.535	16.153	15.534	14.597	3.712784 ± 0.000022	241.020811 ± 0.000466	8.7	24.5
101177265	E2_2999	19 26 55.58	1 17 31.6	16.274	15.488	15.139	14.557	0.641837 ± 0.000008	236.705085 ± 0.001152	5.73	1.8
101180741	E2_2365	19 26 56.86	2 02 06.3	17.057	15.589	14.993	14.103	0.569331 ± 0.000003	237.474741 ± 0.000472	3.80	1.1
101183660	E2_2553	19 26 57.96	1 21 03.8	15.642	14.504	14.024	13.248	9.464590 ± 0.000731	245.172271 ± 0.005533	5.69	0.3

Table 6. continued.

CoRoTid	Winid	Right ascension (J2000.0)	Declination (J2000.0)	*B*	*V*	*R*	*I*	Period(d)	Epoch (HJD-2 454 000)	Length (h)	Depth (%)
101190418	E2_3034	19 27 00.48	1 54 35.9	16.248	15.455	15.092	14.594	2.944843 ± 0.000011	239.298109 ± 0.000309	7.2	25.0
101197456	E2_2459	19 27 03.13	2 08 59.6	16.518	15.195	14.622	13.914	0.295739 ± 0.000001	237.182719 ± 0.000163	1.26	2.3
101199550	E1_3684	19 27 03.90	0 14 51.1	15.705	14.012	13.330	12.372	0.785729 ± 0.000006	237.783379 ± 0.000580	3.00	0.2
101205718	E1_1352	19 27 06.19	0 29 21.5	16.157	14.729	14.205	13.274	30.339189 ± 0.002361	266.615760 ± 0.006101	6.76	0.7
101206902	E2_4232	19 27 06.62	1 15 43.9	16.904	15.953	15.524	15.182	1.684518 ± 0.000004	238.485452 ± 0.000209	2.5	2.4
101212999	E1_5097	19 27 08.94	0 32 00.9	17.132	16.094	15.695	15.034	20.749670 ± 0.000255	257.374145 ± 0.000971	6.8	4.8
101213599	E1_2727	19 27 09.15	−0 05 36.9	15.953	14.972	14.538	13.911	0.59042 ± 0.00010	236.98500 ± 0.000500	1.8	13.5
101232076	E1_0531	19 27 16.12	−0 05 38.3	14.372	13.457	13.069	12.531	0.373297 ± 0.000001	237.300064 ± 0.000280	2.6	2.5
101237431	E1_1891	19 27 18.15	0 34 12.3	15.769	14.749	14.384	13.660	6.060970 ± 0.000039	240.538448 ± 0.000508	6.0	4.3
101245002	E1_4077	19 27 21.06	−0 17 05.3	15.884	15.011	14.627	14.045	5.469796 ± 0.000138	240.800866 ± 0.001938	4.54	0.3
101248929	E2_3063	19 27 22.58	1 16 43.9	17.209	15.863	15.249	14.372	1.880136 ± 0.000069	238.581139 ± 0.003069	1.96	0.1
101254412	E1_5526	19 27 24.66	0 31 29.4	16.853	15.839	15.437	14.693	2.048796 ± 0.000006	238.385189 ± 0.000256	8.2	45.7
101257654	E2_4910	19 27 25.87	1 03 01.0	17.674	16.208	15.613	14.676	0.541751 ± 0.000004	237.393137 ± 0.000599	3.47	0.6
101258066	E1_5728	19 27 26.02	0 41 04.2	17.359	15.822	15.286	14.292	4.291827 ± 0.000027	239.630950 ± 0.000516	3.5	1.5
101259838	E2_1543	19 27 26.68	1 05 46.7	16.309	15.043	14.484	13.698	7.609344 ± 0.000175	244.205604 ± 0.001623	2.16	0.5
101265799	E1_5270	19 27 29.01	−0 24 51.0	16.987	16.074	15.630	15.098	75.520468 ± 0.002939	279.049742 ± 0.002052	10.66	5.4
101271163	E2_4512	19 27 30.98	0 57 01.1	16.947	15.426	14.780	13.913	9.514708 ± 0.000133	243.472995 ± 0.001100	8.2	1.5
101272867	E1_0641	19 27 31.56	−0 10 29.0	15.273	13.819	13.170	12.408	1.995658 ± 0.000045	238.154392 ± 0.001718	6.0	0.3
101275189	E1_4973	19 27 32.37	−0 29 09.3	17.434	16.231	15.627	15.025	7.279587 ± 0.000012	244.496882 ± 0.000135	18.0	10.6
101280276	E2_4809	19 27 34.16	1 27 14.0	17.112	16.117	15.713	14.990	1.656221 ± 0.000006	238.681991 ± 0.000254	2.8	3.4
101283153	E2_5698	19 27 35.21	1 30 53.9	17.529	16.392	15.912	15.122	1.497178 ± 0.000065	238.259525 ± 0.004006	3.62	0.1
101284209	E1_1752	19 27 35.60	0 38 24.4	16.858	15.386	14.833	13.875	0.704843 ± 0.000004	237.687908 ± 0.000507	2.73	0.1
101284287	E1_2904	19 27 35.63	0 09 09.6	15.889	15.034	14.670	14.151	2.375148 ± 0.000009	239.378534 ± 0.000304	6.7	7.2
101286268	E2_0258	19 27 36.35	1 13 09.9	14.150	13.171	12.713	12.043	16.001444 ± 0.000100	248.990835 ± 0.000403	3.89	3.9
101290947	E2_1055	19 27 38.04	1 07 18.6	15.756	14.659	14.142	13.393	2.048782 ± 0.000004	238.693419 ± 0.000167	2.1	4.0
101294080	E1_4581	19 27 39.16	0 05 43.0	16.346	15.546	15.189	14.732	0.765888 ± 0.000004	237.535611 ± 0.000413	3.69	0.7
101296363	E1_2244	19 27 39.98	0 43 00.1	16.329	15.084	14.620	13.799	1.365921 ± 0.000006	238.398759 ± 0.000381	2.9	11.0
101304238	E1_0780	19 27 42.92	0 17 08.2	13.726	13.008	12.686	12.266	1.326786 ± 0.000015	238.199162 ± 0.000094	10.0	1.0
101310684	E1_1894	19 27 45.39	0 44 46.6	16.684	15.050	14.424	13.461	0.557535 ± 0.000006	237.563061 ± 0.000802	4.5	0.35
101310764	E1_0261	19 27 45.42	−0 16 07.5	13.124	12.416	12.077	11.635	2.274738 ± 0.000016	239.141195 ± 0.000559	2.81	0.4
101330506	E1_1242	19 27 54.72	0 46 12.5	16.104	14.666	14.099	13.221	2.545747 ± 0.000039	238.930304 ± 0.001393	1.46	0.8
101330673	E1_4723	19 27 54.81	0 32 37.5	15.039	13.945	13.552	12.851	3.576971 ± 0.000037	239.419112 ± 0.000855	12.3	2.0
101337790	E2_0169	19 27 58.26	1 35 04.8	13.039	12.367	12.180	11.625	1.443336 ± 0.000005	238.054561 ± 0.000269	3.62	8.1
101345254	E1_5007	19 28 01.96	0 25 46.2	15.024	14.090	13.754	13.096	1.970976 ± 0.000007	238.990282 ± 0.000356	5.6	7.0
101361198	E1_1922	19 28 09.68	−0 28 24.4	15.874	15.031	14.627	14.205	0.644797 ± 0.000005	237.634166 ± 0.000591	3.6	28.0
101361346	E1_2335	19 28 09.75	−0 22 00.4	15.649	14.876	14.522	14.085	0.494337 ± 0.000002	237.529343 ± 0.000283	3.45	18.8
101373470	E2_4121	19 28 16.61	1 18 15.6	16.812	15.895	15.480	14.899	0.267900 ± 0.000001	237.051371 ± 0.000321	1.01	2.0
101382355	E1_1033	19 28 20.35	0 16 59.3	14.748	14.017	13.734	13.311	1.368115 ± 0.000084	237.933718 ± 0.000466	10.0	0.09
101386354	E1_0220	19 28 22.00	−0 21 39.9	14.254	12.706	12.037	11.275	1.487714 ± 0.000024	238.494342 ± 0.001306	3.62	0.1
101388668	E1_3418	19 28 22.93	0 16 27.7	16.948	15.622	15.079	14.336	27.888839 ± 0.000548	252.094998 ± 0.001580	14.0	8.5
101393506	E2_3665	19 28 24.96	1 13 45.9	16.698	15.815	15.431	15.108	16.55723 ± 0.000100	239.653327 ± 0.000457	6.1	18.8
101403809	E1_3001	19 28 29.26	0 42 54.1	16.125	15.165	14.834	14.156	0.659926 ± 0.000006	237.6400 ± 0.00100	3.0	3.7
101437920	E1_2540	19 28 43.32	−0 04 36.2	16.642	15.392	14.908	14.186	0.404962 ± 0.000001	237.398080 ± 0.000306	2.36	0.4
101445950	E1_1648	19 28 46.62	−0 15 20.8	15.854	14.811	14.332	13.800	32.25590 ± 0.000338	254.125751 ± 0.000703	2.8	5.5
101458754	E1_1422	19 28 51.83	0 09 25.7	15.924	14.566	14.024	13.301	17.942907 ± 0.001778	247.182508 ± 0.007299	7.21	0.3
101529250	E1_5157	19 29 20.93	0 09 30.4	17.428	16.236	15.689	15.011	0.406438 ± 0.000001	237.275900 ± 0.000229	3.0	31.0
101543261	E1_5020	19 29 26.87	0 10 58.5	17.738	16.291	15.869	15.296	0.318524 ± 0.000001	237.308377 ± 0.000175	3.0	6.7
101551987	E1_1277	19 29 30.53	0 00 50.0	15.391	14.406	13.997	13.455	3.136944 ± 0.000006	239.949132 ± 0.000156	4.5	19.0
101572706	E1_0908	19 29 38.48	−0 03 36.6	14.577	13.791	13.455	12.999	0.432330 ± 0.000001	237.694656 ± 0.000216	4.5	11.0
101579613	E1_1273	19 29 41.18	−0 12 56.5	15.144	14.358	13.990	13.562	3.681288 ± 0.000022	240.144745 ± 0.000464	7.44	4.5
101589332	E1_5168	19 29 44.97	0 38 26.4	17.108	15.986	15.509	14.815	80.738482 ± 0.003673	281.516278 ± 0.002978	7.06	10.8
101627640	E1_4050	19 30 03.19	0 23 19.4	16.519	15.567	15.167	14.528	0.626306 ± 0.000011	237.270000 ± 0.005000	3.88	1.4
101633581	E1_0747	19 30 06.20	−0 07 25.1	15.775	14.151	13.488	12.665	8.996041 ± 0.000512	245.104033 ± 0.004071	4.41	0.1
101644400	E1_3268	19 30 11.64	−0 00 27.8	16.257	15.291	14.908	14.345	5.300527 ± 0.000071	240.782635 ± 0.001001	3.17	0.7
101650673	E1_2268	19 30 15.36	0 11 32.2	16.325	15.271	15.457	14.965	0.433146 ± 0.000001	237.311194 ± 0.000266	4.0	8.9
101657424	E1_5665	19 30 18.82	−0 04 17.6	16.584	14.891	14.147	13.145	0.954974 ± 0.000012	237.747480 ± 0.001064	1.40	0.2